NUS
National University
of Singapore

THE PHYSICS OF BLACK SATURN

Foo Yun Shuen Cassandra
A0102427U
Supervisor: Dr. Kenneth Hong Chong Ming

Honours Project in Physics (Astrophysics)
AY2015/16
Faculty of Science
Department of Physics

Acknowledgments

First and foremost, I would like to thank my supervisor, Dr. Kenneth Hong Chong Ming, for his unyieldingly patient guidance throughout the course of this project. I could not have climbed the intimidatingly steep learning curve involved in understanding black hole research and using Maple for laborious calculations without the revelations he provided during our meetings and the efficiency with which he replied to convolutedly phrased questions in emails.

I am thankful to Ren Jie, my fellow newcomer to the world of black hole research under Dr. Hong's supervision, with whom I shared many confusions, discussions as well as 'Eureka!' moments. I also thank all my peers and friends for their unrelenting support and encouragement, as well as my family for their love and concern for me over the increasing darkness of the circles around my eyes.

Last but not least, I thank God, my Lord and Saviour, for being my unfailing source of strength and comfort, and for His incredible thoughtfulness in remembering the time I first read about black holes in an encyclopedia and told Him, "How I'd love to study this in University!", and so here I am.

Abstract

We cover the steps involved in the study of the physics of an exact stationary asymptotically flat (4+1)-dimensional vacuum black hole solution describing the black Saturn system: a spherical (4+1)-dimensional black hole surrounded by a (4+1)-dimensional black ring, balanced by angular momentum. The black Saturn, discovered by Elvang and Figueras (2007), is the very first balanced multiple-black-hole solution to be obtained. It exhibits two-fold continuous non-uniqueness for fixed mass and angular momentum measured at infinity as well as the General Relativistic phenomenon of rotational frame-dragging by one black object on the other. Possible generalisations include doubly spinning, charged as well as multiple-ringed black Saturn configurations.

List of Figures

Contents

Chapter 1

Introduction

1.1 Motivations

A black hole is a region of spacetime deformed by such a compact mass that nothing, not even light, can escape it. Extensive research has been done on black holes in (3+1)-dimensional General Relativity, given that we live in an observably four-dimensional world. However, as it turns out, four-dimensional spacetime has been restricting the possible solutions to Einstein's field equations, and in more recent years, attention has been turned to the study of black holes in higher-dimensional spacetime. The motivation for such an interest is the opportunity to analyse interesting physics phenomena to give us a more comprehensive understanding of General Relativity and other higher-dimensional theories, as well as the opportunity to study the existence of various novel features of higher-dimensional black holes.

(i) Topologically non-spherical black holes

Hawking's theorem of black hole topology (1972) [1] asserts that in the case of four-dimensional asymptotically flat black holes satisfying the suitable energy conditions, the temporal cross-sections of the event horizon are spherical, i.e., of topology S^2. A few examples are the Schwarzschild (1916) and Kerr (1963) black hole solutions. Generalising to n-dimensional spacetime, we get the Tangherlini (1963) and Myers-Perry (1986) black hole solutions respectively, which have temporal cross-sections of higher dimensional spheres. However, in 2002, Roberto Emparan and Harvey Reall discovered the first black hole solution with a non-spherical event horizon, namely one of topology $S^1 \times S^2$: a (4+1)-dimensional black ring [2]. This solution will be described in detail in Section 2.3.

(ii) Violation of black hole uniqueness theorem

The uniqueness theorem of black holes [3] states that stationary, asymptotically flat vacuum black holes are uniquely determined by the asymptotically conserved physical quantities of mass, angular momentum and charge. In other words, for every combination of mass, angular momentum and charge measured at infinity, there is only one possible black hole solution. However, in five dimensions and above, it has been proven that the uniqueness theorem holds only for static cases [4] and breaks down for stationary cases [5]. Consequently, for the same mass, angular momentum and charge measured at infinity, there exist several black hole solutions. In addition, phase transitions from one black hole to another are allowed, implying the classical instability of certain higher-dimensional black holes. Violation of the uniqueness theorem will be further elaborated upon in Section 2.6.

(iii) Balanced multiple-black-hole solutions

Searching for balanced multiple-black-hole solutions has long been of interest but also found to be difficult. In four-dimensional spacetime, the simplest way to achieve a balanced static configuration between two Schwarzschild black holes, for instance, is by adding enough electric charge to each hole such that electromagnetic repulsion exactly cancels gravitational attraction. Generalised to a multiple-black-hole solution, this gives the extremal multi-Reissner Nordström non-vacuum black hole solution [6], where mass and charge become equal, i.e., they are no longer independent of one another but are subfamilies of the solution. For a vacuum solution, that is, without charge, rotation is the only candidate for keeping black holes apart. However, for the four-dimensional double Kerr solution [7], spin-spin interaction is not sufficiently strong to keep the system balanced; a topological defect is required to keep the black holes apart and prevent collapse. The multi-Kerr black hole spacetime thus suffers from conical singularities, either a rod or strut between the holes providing pressure, or strings extending to infinity providing tension. Such a solution is irregular which is undesirable.

In 2007, Elvang and Figueras superimposed two higher-dimensional black hole solutions to obtain the very first exact balanced asymptotically-flat multiple-black-hole solution known as the black Saturn solution [8]. The black Saturn system comprises a five-dimensional Myers-Perry black hole and a balanced five-dimensional Emparan-Reall black ring, which rotates such that the overall angular momentum of the system generates the centrifugal force necessary to keep the configuration in equilibrium. Black Saturn is thus the first multiple-black-hole vacuum solution requiring no conical singularity in order to achieve balance.

1.2 Organisation of thesis

This thesis mainly studies the five-dimensional black Saturn solution. The organisation of the thesis is as follows. Chapter 2 contains a review of two well-known asymptotically flat vacuum black hole solutions in five dimensions, namely the Myers-Perry black hole and the Emparan-Reall black ring, with the focus being on the physical properties of these solutions. Chapter 3 introduces the black Saturn solution whereas Chapter 4 is an analysis of the solution where the physics of the black Saturn metric is extracted and accounted for. We end off with the future outlook for the study of black Saturn solutions and other higher-dimensional black hole solutions in Chapter 5.

Chapter 2

Known Five-Dimensional Black Hole Solutions

2.1 Introduction

In this chapter, we will review two well-known asymptotically flat vacuum black hole solutions, namely the five-dimensional singly rotating Myers-Perry black hole and the Emparan-Reall black ring, which together form the black Saturn system. Before that, however, there are several things to take note of, as well as key ideas that need to be introduced.

Canonical form of a metric

The generic form for any metric is typically

$$ds^2 = \sum_{a,b=1}^{D} g_{ab} dx^a dx^b \,. \tag{2.1}$$

However, for vacuum solutions in stationary and axisymmetric spacetime [9], we can find a coordinate system such that it takes the canonical form

$$ds^2 = \sum_{i,j=1}^{D-2} G_{ij} dx^i dx^j + f(d\rho^2 + dz^2) \,, \tag{2.2}$$

where

$$\rho = \sqrt{|\det(G_{ij})|} \,, \tag{2.3}$$

assuming that $\det(G_{ij})$ is not a constant. G_{ij} and f are functions of only ρ and z, which are called the Weyl coordinates [10], and f is known as the

conformal factor. The canonical form of the metric is useful for calculating rod structures.

Rod structures

The rod structure of a solution is characterised by rods, given by rod endpoints on the z-axis with $\rho = 0$, and the associated rod vectors. Let a solution $G_{ij}(\rho, z)$ be given by $N+1$ rods defined by $N+1$ vectors $v_{(k)}$ which meet in the z-values $a_1 < a_2 < ... < a_N$. We introduce the notation $a_0 = -\infty$ and $a_{N+1} = \infty$ for the equations below to be more compactly written. The solution $G_{ij}(\rho, z)$ thus has $N+1$ rods $[a_{k-1}, a_k]$ with $k = 1, ..., N+1$ and must satisfy this equation [9]:

$$G_{ij}(0, z)v_{(k)} = 0 \quad \text{for } z \in [a_{k-1}, a_k],\ k = 1, ..., N+1\,, \tag{2.4}$$

with $v_{(k)} \neq 0$ for all $k = 1, ...N+1$. In other words, the direction $v_{(k)}$ of a given rod with rod interval $[a_{k-1}, a_k]$ is the zero eigenvalue eigenvector of G_{ij} at $\rho = 0$. Since $v_{(k)}$ is defined as an eigenvector, it is only defined up to a (non-zero) multiplicative factor. Both static and stationary black hole solutions can be specified by rod structures but in this thesis we will focus on the rod structures of stationary solutions.

There are two types of rods that are relevant to this thesis: spacelike rods and timelike rods, which have positive and negative values, respectively, for the following expression [11] that is a constant within the interior of each individual rod:

$$\frac{|v_{(k)}|^2}{\rho^2 f}\,. \tag{2.5}$$

A spacelike rod represents an axis of rotation and is associated with the angle swept out by an object orbiting around the black hole, i.e., the periodicity of the solution:

$$\triangle\eta = 2\pi \lim_{\rho\to 0} \sqrt{\frac{\rho^2 f}{|v_{(k)}|^2}}\,. \tag{2.6}$$

The periodicity $\triangle\eta$ of a regular solution is always 2π. The physical interpretation for an irregular solution with non-2π periodicity is that black hole configuration cannot be balanced without conical singularties appearing in the spacetime. In addition, the direction of a spacelike rod must not contain a time component, or else pathological closed timelike curves will be present. We define the Euclidean surface gravity of a spacelike rod as

$$\kappa_E = \lim_{\rho\to 0} \sqrt{\frac{|v_{(k)}|^2}{\rho^2 f}}\,, \tag{2.7}$$

such that $\triangle\eta = 2\pi/\kappa_E$. Correspondingly, we define the (non-Euclidean) surface gravity of a timelike rod as

$$\kappa = \lim_{\rho\to 0}\sqrt{-\frac{|v_{(k)}|^2}{\rho^2 f}}\,. \tag{2.8}$$

A timelike rod represents the event horizon of a black hole and is associated with the temperature measured at the event horizon, such that $T = \kappa/(2\pi)$, i.e.,

$$T = \frac{1}{2\pi}\lim_{\rho\to 0}\sqrt{-\frac{|v_{(k)}|^2}{\rho^2 f}}\,. \tag{2.9}$$

In the schematic diagrams of rod structures throughout this thesis, solid lines denote spacelike rods and dotted lines denote timelike rods.

Physical quantities

Throughout this thesis, unless otherwise stated, the quantities of mass M and angular momentum J are measured at infinity, whereas the quantities of angular velocity Ω and temperature T are measured at the event horizon, which has an area of A_H. The index $i = BH, BR$ specifies the black object to which the property belongs: BH refers to the Myers-Perry black hole whereas BR refers to the Emparan-Reall black ring. For example, M_{BH} means 'mass of Myers-Perry black hole measured at infinity'.

Mass M and angular momentum J can be calculated by applying the asymptotic coordinate transformation $\rho = \rho(r,\theta)\,,\ z = z(r,\theta)$ to the metric and Taylor expanding for $r \to \infty$. For solutions that asymptote to five-dimensional Minkowski-space, the corrections to the metric are related to M and J [9] as follows:

$$g_{tt} = -1 + \frac{8M}{3\pi}\frac{1}{r^2} + \mathcal{O}\left(\frac{1}{r^4}\right), \tag{2.10}$$

$$g_{t\psi} = -\frac{4J_\psi}{\pi}\frac{\sin^2\theta}{r^2}\left(1+\mathcal{O}\left(\frac{1}{r^2}\right)\right), \quad g_{t\phi} = -\frac{4J_\phi}{\pi}\frac{\cos^2\theta}{r^2}\left(1+\mathcal{O}\left(\frac{1}{r^2}\right)\right). \tag{2.11}$$

Event horizon area A_H can be calculated using the metric g^{Hor} of a spatial cross-section of the horizon of a solution, which may be obtained from the complete metric by setting $dt = dY = 0$, where Y is the coordinate for which an expression can be substituted to give the location of the event horizon,

e.g. $dt = dr = 0$ and $r = r_+$ (2.17) for the Myers-Perry black hole. We then use

$$A_H = \iiint \sqrt{|\det(g^{Hor})|} dX d\phi d\psi \,, \tag{2.12}$$

integrating ϕ and ψ from 0 to 2π, and X over an appropriate range as well.

2.2 Myers-Perry black hole solution

The Myers-Perry (MP) solution is a generalisation of the four-dimensional Kerr solution to arbitrary higher dimensions, and it is non-trivial due to the possibility of rotation in different planes in higher-dimensional spacetimes. This vacuum solution is asymptotically flat, non-static but stationary and has an event horizon of topology S^3 in five-dimensional (5D) spacetime. The metric of the 5D MP black hole [11] is

$$\begin{aligned} ds^2 = &-dt^2 + \frac{2m}{\Sigma}(dt - a\sin^2\theta\, d\psi - b\cos^2\theta\, d\phi)^2 + \Sigma\left(\frac{dr^2}{\Delta} + d\theta^2\right) \\ &+ (r^2 + a^2)\sin^2\theta\, d\psi^2 + (r^2 + b^2)\cos^2\theta\, d\phi^2 \,, \end{aligned} \tag{2.13}$$

where

$$\Sigma = r^2 + a^2\cos^2\theta + b^2\sin^2\theta \,, \quad \Delta = r^2\left(1 + \frac{a^2}{r^2}\right)\left(1 + \frac{b^2}{r^2}\right) - 2m \,, \tag{2.14}$$

with m being the parameter for mass and a and b being the parameters for rotation in the azimuthal directions ψ and ϕ respectively.

For the purposes of this thesis, it is sufficient to focus on the singly rotating MP black hole, i.e., $b = 0$ and the black hole is rotating only in the ψ-direction. The metric (2.13) with (2.14) then becomes

$$\begin{aligned} ds^2 = &-dt^2 + \frac{2m}{\Sigma}(dt - a\sin^2\theta\, d\psi)^2 + \Sigma\left(\frac{dr^2}{\Delta} + d\theta^2\right) \\ &+ (r^2 + a^2)\sin^2\theta\, d\psi^2 + r^2\cos^2\theta\, d\phi^2 \,, \end{aligned} \tag{2.15}$$

where

$$\Sigma = r^2 + a^2\cos^2\theta, \quad \Delta = r^2 - 2m + a^2 \,. \tag{2.16}$$

Note that $a = 0$ in addition to $b = 0$ reduces (2.15) to the 5D Tangherlini solution, and setting $m = 0$ as well returns us 5D Minkowski spacetime.

The location of the event horizon of the MP black hole is given by the expression of r for which the inverse metric component g^{rr} vanishes, i.e., $\Delta(r_+) = 0$ [11]:

$$r_+ = \sqrt{2m - a^2} \,. \tag{2.17}$$

2.2.1 Rod structure

To express the metric (2.15) with (2.16) in canonical form (2.2) with $D = 5$ and indices $t = 1$, $\phi = 2$ and $\psi = 3$, the following transformation [9] is needed:

$$\rho = \frac{1}{2} r \sin 2\theta \sqrt{\Delta} = \frac{1}{2} r \sin 2\theta \sqrt{r^2 - 2m + a^2}\,, \tag{2.18}$$

$$z = \frac{1}{4}(2r^2 - 2m + a^2)\cos 2\theta \quad \text{with}\, b = 0. \tag{2.19}$$

The Weyl coordinate ρ (2.18) is determined by computing

$$\begin{aligned} \det(G_{ij}) &= r^2 \sin^2\theta \cos^2\theta(-r^2 + 2m - a^2) \\ &= -\frac{1}{4} r^2 \sin^2 2\theta (r^2 - 2m + a^2)\,, \end{aligned} \tag{2.20}$$

and demanding that

$$\det(G_{ij}) = -\rho^2\,. \tag{2.21}$$

The conformal factor for the metric is

$$f = \frac{2[2r^2 + a^2(1 + \cos 2\theta)]}{[(a^2 - 2m)(1 + \cos 2\theta) + 2r^2][(a^2 - 2m)(1 - \cos 2\theta) + 2r^2]}\,. \tag{2.22}$$

Solving for $\rho = 0$, we find that the rod structure for the MP black hole has two turning points located at ($\rho = 0$, $z = z_1 \equiv -\alpha$) or ($r = r_+$, $\theta = \pi/2$) and ($\rho = 0$, $z = z_2 \equiv \alpha$) or ($r = r_+$, $\theta = 0$), where

$$\alpha = \frac{2m - a^2}{4}\,, \tag{2.23}$$

and r_+ is defined in (2.17). The two turning points partition the z-axis into three rods, whose directions $v_{(k)}$, $k = 1, 2, 3$ can be obtained by substituting $\theta = \pi/2$, $r = r_+$ and $\theta = 0$ respectively into the matrix G and calculating the null eigenvector for the resulting matrix.

Figure 2.1 is a schematic diagram representing the rod structure for the MP black hole:

- **Rod 1** (leftmost rod) is a semi-infinite spacelike rod at ($\rho = 0$, $z \le z_1$) or ($r \ge r_+$, $\theta = \pi/2$) with direction $v_{(1)} = (0, 1, 0)$.
- **Rod 2** is a finite timelike rod at ($\rho = 0$, $z_1 \le z \le z_2$) or ($r = r_+$, $0 \le \theta \le \pi/2$) with direction $v_{(2)} = \frac{1}{\kappa}(1, 0, \Omega)$. The surface gravity κ of Rod 2 and angular velocity Ω of the MP black hole are given by:

$$\kappa = \frac{1}{2m}\sqrt{2m - a^2}\,, \tag{2.24}$$

$$\Omega = \frac{a}{2m} \quad \text{in the } \psi\text{-direction.} \tag{2.25}$$

· **Rod 3** (rightmost rod) is a semi-infinite spacelike rod at ($\rho = 0$, $z \geq z_2$) or ($r \geq r_+$, $\theta = 0$) with direction $v_{(3)} = (0, 0, 1)$.

The Euclidean surface gravities κ_E (2.7) of the spacelike rods 1 and 3 are as follows:

$$\kappa_{E,1} = 1\,, \quad \kappa_{E,3} = 1\,. \tag{2.26}$$

The unity of both values of κ_E implies that both the angular coordinates ϕ and ψ have standard periodicities of 2π.

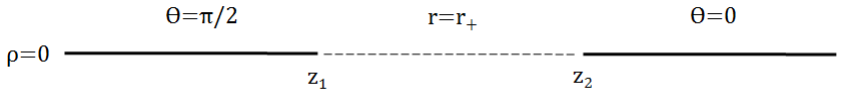

Figure 2.1: Schematic diagram of MP rod structure

2.2.2 Physical quantities

We have all we need to obtain the expressions for the physical quantities of the MP black hole.

The timelike rod of the MP black hole, Rod 2, gives us the angular velocity (2.25) as well as the temperature of the MP black hole, since $T = \kappa/(2\pi)$:

$$T = \frac{1}{4\pi m}\sqrt{2m - a^2}\,, \tag{2.27}$$

whereas event horizon area can be found using (2.12) with $Y = r$ and by integrating $X = \theta$ from 0 to $\pi/2$:

$$A_H = 4\pi^2 m\sqrt{2m - a^2}\,. \tag{2.28}$$

In the asymptotic region, i.e., $\sqrt{\rho^2 + z^2} \to \infty$, with $z/\sqrt{\rho^2 + z^2}$ being finite, Taylor expansion of each non-zero component of the metric G_{ij} gives:

$$G_{tt} = -1 + \frac{2m}{r^2} + \mathcal{O}\left(\frac{1}{r^4}\right), \quad G_{t\psi} = -\frac{2ma\sin^2\theta}{r^2} + \mathcal{O}\left(\frac{1}{r^4}\right), \quad G_{t\phi} = 0\,, \tag{2.29}$$

hence the mass and angular momentum of the MP black hole can be calculated by equating (2.29) with (2.10) and (2.11):

$$M = \frac{3\pi m}{4}\,, \tag{2.30}$$

$$J_\psi = \frac{\pi}{2} ma \,, \quad J_\phi = 0 \,. \tag{2.31}$$

Note that $J_\phi = 0$ since the MP black hole is singly rotating and $b = 0$.

We introduce fixed mass reduced parameters [8] computed as follows for 5D metrics, which allow us to compare physical properties of configurations with the same mass M:

$$\begin{aligned} \omega &= \sqrt{\frac{8M}{3\pi}}\Omega \,, \quad \tau = \sqrt{\frac{32\pi M}{3}} T \,, \\ a_H &= \frac{3}{16}\sqrt{\frac{3}{\pi M^3}} A_H \,, \quad j = \frac{3}{4}\sqrt{\frac{3\pi}{2M^3}} J \,. \end{aligned} \tag{2.32}$$

Thus, we obtain, from (2.25), (2.27), (2.28) and (2.31):

$$\omega = \sqrt{\frac{a^2}{2m}} \,, \quad \tau = \sqrt{\frac{2m - a^2}{2m}} \,, \tag{2.33}$$

$$a_H = 2\sqrt{\frac{2m - a^2}{m}} \,, \quad j = j_\psi = \sqrt{\frac{a^2}{2m}} \,, \quad j_\phi = 0 \,. \tag{2.34}$$

The reduced angular velocity and temperature are normalised such that $\omega = 1$ for the maximally rotating (singular) MP black hole ($j = 1$) and $\tau = 1$ for the 5D Tangherlini black hole ($j = 0$). In fact, we note that $\omega = j$ due to the choice made for these reduced parameters [8].

2.3 Emparan-Reall black ring solution

The 5D Emparan-Reall (ER) black ring is a black hole with a horizon topology of $S^1 \times S^2$. The metric of the S^1 singly rotating solution (no S^2 rotation) [11] is given by:

$$\begin{aligned} ds^2 = &-\frac{F(y)}{F(x)}\left[dt - \varkappa\sqrt{\frac{2\lambda(\lambda-\mu)(1+\lambda)}{1-\lambda}}\frac{1+y}{F(y)}d\psi\right]^2 \\ &+\frac{2\varkappa^2 F(x)}{(x-y)^2}\Bigg\{ -\frac{G(y)}{F(y)}d\psi^2 + \frac{G(x)}{F(x)}d\phi^2 \\ &\qquad + \frac{(1-\mu)^2}{1-\lambda}\left[\frac{dx^2}{G(x)} - \frac{dy^2}{G(y)}\right]\Bigg\} \,, \end{aligned} \tag{2.35}$$

where

$$\begin{aligned} F(x) &= 1 + \lambda x \,, \quad G(x) = (1-x^2)(1+\mu x) \,, \\ F(y) &= 1 + \lambda y \,, \quad G(y) = (1-y^2)(1+\mu y) \,. \end{aligned} \tag{2.36}$$

The parameters λ and μ are dimensionless and must lie in the range

$$0 \leq \mu \leq \lambda < 1\,. \tag{2.37}$$

When $\lambda = \mu = 0$, (2.35) with (2.36) becomes

$$ds^2 = -dt^2 + \frac{2\varkappa^2}{(x-y)^2}\left[(y^2-1)d\psi^2 + (1-x^2)d\phi^2 + \frac{dx^2}{1-x^2} - \frac{dy^2}{1-y^2}\right], \tag{2.38}$$

which is the metric for flat spacetime in the so-called ring coordinates [11]. The parameter $\varkappa > 0$ has dimensions of length and sets the scale of the solution. The coordinates x and y take the values

$$-1 \leq x < 1, \quad -\infty < y \leq -1\,, \tag{2.39}$$

and hence ensure that $g_{\psi\psi} > 0$. The location of the event horizon of the ER black ring is at $y = -1/\mu$, where $G(y) = 0$.

A commonly used geometric visualisation for the ER black ring is the toroidal shape of a donut, with the circular cross-section of the toroid not comprised of a continuous set of points but a sequence of S^2 spheres. Rotating about the axis running through the hole in the toroid represents S^1 rotation; rotation of the sequence of spheres about their own individual axes represents S^2 rotation. Another way to visualise the black ring is by using the ring coordinate diagram as in Figure 2.2: S^1 rotation is given by selecting a pair of circles symmetric in the y-axis and rotating them out of the plane of the page.

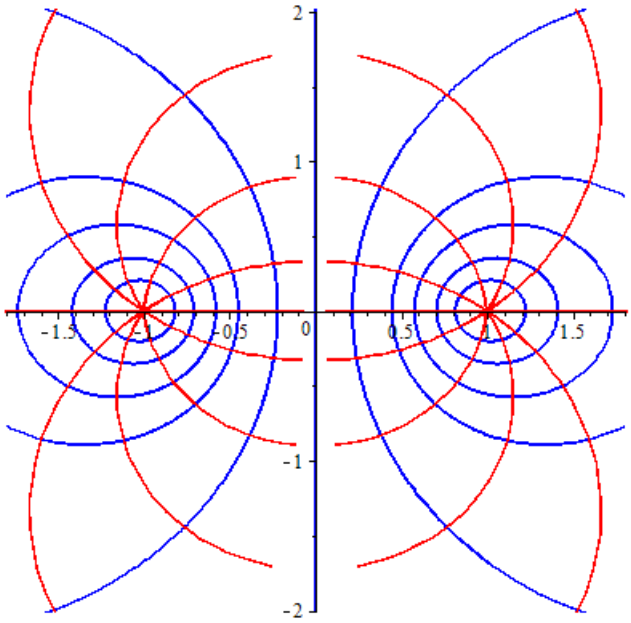

Figure 2.2: Emparan-Reall ring coordinate diagram

2.3.1 Rod structure

To express the metric (2.35) in canonical form (2.2) with $D = 5$ and indices $t = 1\,, \phi = 2$ and $\psi = 3$, the following transformation [9] is needed:

$$\begin{aligned} \rho &= \frac{2\varkappa^2\sqrt{-G(y)G(x)}}{(x-y)^2} \\ &= \frac{2\varkappa^2\sqrt{(1-x^2)(y^2-1)(1+\mu x)(1+\mu y)}}{(x-y)^2}\,, \end{aligned} \tag{2.40}$$

$$z = \frac{\varkappa^2(1-xy)[2+\mu(x+y)]}{(x-y)^2}\,. \tag{2.41}$$

The Weyl coordinate ρ is determined by computing

$$\det(G_{ij}) = -\frac{4\varkappa^4(1-x^2)(y^2-1)(1+\mu x)(1+\mu y)}{(x-y)^4}\,, \tag{2.42}$$

and demanding that

$$\det(G_{ij}) = -\rho^2\,. \tag{2.43}$$

The conformal factor for the metric is

$$f = \frac{2(x-y)}{\varkappa^2(\mu xy+\mu x+\mu y-\mu+2)(\mu xy-\mu x-\mu y-\mu-2)} \times \frac{(1+\lambda x)}{\mu xy+\mu+x+y}\,. \tag{2.44}$$

Solving for $\rho = 0$, we find that the rod structure for the ER black ring has three turning points located at ($\rho = 0$, $z = z_1 \equiv -\mu\varkappa^2$) or ($x = -1$, $y = -1/\mu$), ($\rho = 0$, $z = z_2 \equiv \mu\varkappa^2$) or ($x = 1$, $y = -1/\mu$), and ($\rho = 0$, $z = z_3 \equiv \varkappa^2$) or ($x = 1$, $y = -1$). These three turning points partition the z-axis into four rods, whose directions $v_{(k)}$, $k = 1, 2, 3, 4$ can be obtained by substituting $x = -1$, $y = -1/\mu$, $x = 1$ and $y = -1$ respectively into the matrix G and calculating the null eigenvector for the resulting matrix.

Figure 2.3 is a schematic diagram representing the rod structure for the ER black ring:

- **Rod 1** (leftmost rod) is a semi-infinite spacelike rod at ($\rho = 0$, $z \le z_1$) or ($x = -1$, $-1/\mu \le y < -1$) with direction $v_{(1)} = (0, 1, 0)$.

- **Rod 2** is a finite timelike rod at ($\rho = 0$, $z_1 \le z \le z_2$) or ($-1 \le x \le 1$, $y = -1/\mu$) with direction $v_{(2)} = \frac{1}{\kappa}(1, 0, \Omega)$. The surface gravity κ of Rod 2 and angular velocity Ω of the S^1-rotating ER black ring are given by:

$$\kappa = \frac{(1-\lambda)(1+\mu)}{4\varkappa(1-\mu)}\sqrt{\frac{2}{\lambda\mu(1+\lambda)}}\,, \tag{2.45}$$

$$\Omega = \frac{1}{2\varkappa(1-\mu)}\sqrt{\frac{2(1-\lambda)(\lambda-\mu)}{\lambda(1+\lambda)}} \quad \text{in the } \psi\text{-direction.} \tag{2.46}$$

- **Rod 3** is a finite spacelike rod at ($\rho = 0$, $z_2 \le z \le z_3$) or ($x = 1$, $-1/\mu \le y \le -1$) with direction $v_{(3)} = \frac{1}{\kappa_{E,3}}(0, 1, 0)$. The Euclidean surface gravity $\kappa_{E,3}$ of Rod 3 is given by:

$$\kappa_{E,3} = \frac{1+\mu}{1-\mu}\sqrt{\frac{1-\lambda}{1+\lambda}}\,. \tag{2.47}$$

- **Rod 4** (rightmost rod) is a semi-infinite spacelike rod at ($\rho = 0$, $z \ge z_3$) or ($-1 < x \le 1$, $y = -1$) with direction $v_{(4)} = (0, 0, 1)$.

The Euclidean surface gravities κ_E (2.7) of the spacelike rods 1 and 4 are as follows:

$$\kappa_{E,1} = 1\,, \quad \kappa_{E,4} = 1\,, \tag{2.48}$$

thus both the angular coordinates ϕ and ψ have standard periodicities of 2π.

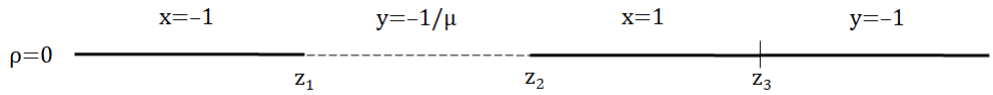

Figure 2.3: Schematic diagram of ER black ring rod structure

To eliminate the possibility of the solution bearing conical singularities, we need to ensure that Rods 1 and 3, which have the same direction, have the same Euclidean surface gravities, i.e., $\kappa_{E,1} = \kappa_{E,3}$. We thus impose $\kappa_{E,3} = 1$ to obtain the balance condition

$$\lambda = \frac{2\mu}{\mu^2 + 1}\,. \tag{2.49}$$

2.3.2 Physical quantities

We have all we need to obtain the expressions for the physical quantities of the ER black ring.

The timelike rod of the ER black ring, Rod 2, gives us the angular velocity (2.46) and the surface gravity associated with it gives the temperature of the ER black ring because of the relation $T = \kappa/(2\pi)$:

$$T = \frac{1}{8\varkappa\pi}\frac{1-\mu}{\mu}\,. \tag{2.50}$$

Using (2.12) with $Y = y$ and by integrating $X = x$ from -1 to 1, the event horizon area of the black ring is found to be

$$A_H = \frac{32\varkappa^3\pi\mu^2}{1-\mu}\,. \tag{2.51}$$

In the asymptotic region, i.e., $\sqrt{\rho^2+z^2} \to \infty$, with $z/\sqrt{\rho^2+z^2}$ being finite, Taylor expansion of each non-zero component of the metric G_{ij} gives:

$$\begin{aligned} G_{tt} &= -1 + \frac{8\varkappa^2\mu}{(1-\mu)r^2} + \mathcal{O}\left(\frac{1}{r^4}\right), \\ G_{t\psi} &= \frac{-8\varkappa^3\mu\sin^2\theta}{r^2}\left(\frac{1+\mu}{1-\mu}\right)^{3/2}, \\ G_{t\phi} &= 0\,. \end{aligned} \tag{2.52}$$

Note that the balance condition (2.49) has been imposed. By equating (2.29) with (2.10) and (2.11), the mass and angular momentum in the ψ-direction are

$$M = \frac{3\varkappa^2\pi\mu}{1-\mu}\,, \tag{2.53}$$

$$J = 2\varkappa^3\pi\mu\left(\frac{1+\mu}{1-\mu}\right)^{3/2}. \tag{2.54}$$

Using (2.32), the fixed mass reduced parameters for (2.46), (2.50), (2.51) and (2.54) are:

$$\begin{aligned} \omega &= \sqrt{\frac{2\mu}{1+\mu}}\,, \quad \tau = \sqrt{\frac{1-\mu}{2\mu}}\,, \\ a_H &= 2\sqrt{\mu(1-\mu)}\,, \quad j = \frac{1}{2}\sqrt{\frac{(1+\mu)^3}{2\mu}}\,. \end{aligned} \tag{2.55}$$

Plotting reduced event horizon area a_H against reduced angular momentum j in Figure 2.4, we see that the ER black ring has two types, as shown by the two branches in the 'phase diagram': fat rings and thin rings; fat rings are on the lower branch while thin rings are on the upper branch. Their shapes can be visualised as in Figure 2.5.

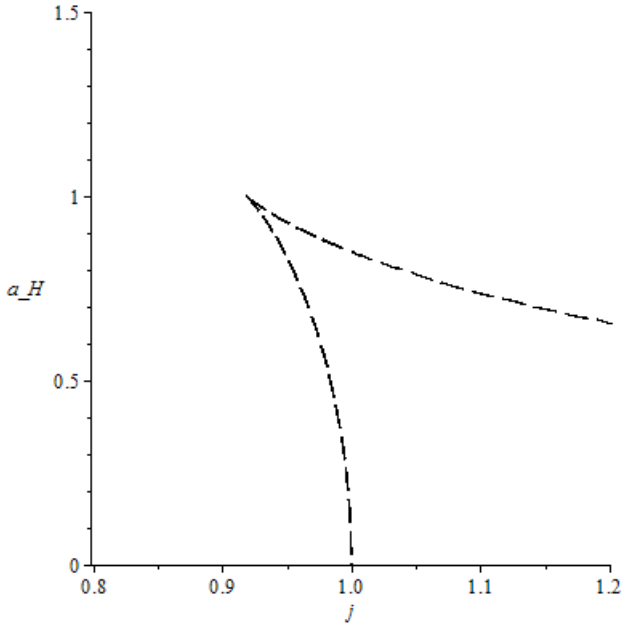

Figure 2.4: Violation of Uniqueness Theorem by ER black rings

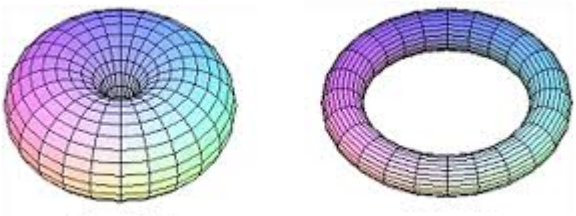

Figure 2.5: Visualisation of fat and thin rings [12]

If we include the graph for the MP black hole as well, we can see in Figure 2.6 that for a given range of parameters for angular momentum, there exist 3 different black hole solutions: two 5D black ring solutions: a fat black ring and thin black ring solution, and a 5D MP solution. At infinity, there is no way to differentiate these solutions.

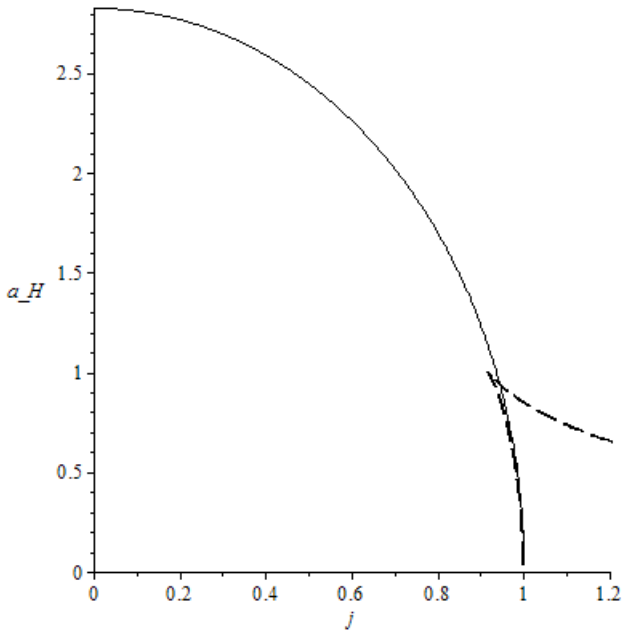

Figure 2.6: Violation of Uniqueness Theorem by MP black hole alongside ER black rings: The solid black line represents the MP black hole and the dashed black line represents the ER black rings.

Chapter 3

Black Saturn solution

In this chapter, we introduce and analyse the ψ-rotating black Saturn solution comprised of an MP black hole and an ER black ring, in order to extract expressions for the physical quantities of black Saturn.

3.1 The metric

The black Saturn metric written in canonical form [8] is given as

$$ds^2 = -\frac{H_y}{H_x}\left[dt + \left(\frac{\omega_\psi}{H_y} + q\right)d\psi\right]^2 + H_x\left\{k^2 P(d\rho^2 + dz^2) + \frac{G_y}{H_y}d\psi^2 + \frac{G_x}{H_x}d\phi^2\right\}. \tag{3.1}$$

Note that the conformal factor f has been written as $k^2 H_x P$, where k is a constant and $G_{x,y}$, $H_{x,y}$ and P are functions of the Weyl coordinates ρ and z. The metric (3.1) involves the functions

$$G_x = \frac{\rho^2\mu_4}{\mu_3\mu_5}\,, \tag{3.2}$$

$$G_y = \frac{\mu_3\mu_5}{\mu_4}\,, \tag{3.3}$$

$$P = (\mu_3\mu_4 + \rho^2)^2(\mu_1\mu_5 + \rho^2)(\mu_4\mu_5 + \rho^2)\,, \tag{3.4}$$

and

$$\begin{aligned} H_x &= F^{-1}[M_0 + c_1^2 M_1 + c_2^2 M_2 + c_1 c_2 M_3 + c_1^2 c_2^2 M_4]\,, \\ H_y &= F^{-1}\frac{\mu_3}{\mu_4}\left[M_0\frac{\mu_1}{\mu_2} - c_1^2 M_1\frac{\rho^2}{\mu_1\mu_2} - c_2^2 M_2\frac{\mu_1\mu_2}{\rho^2} + c_1 c_2 M_3 + c_1^2 c_2^2 M_4\frac{\mu_2}{\mu_1}\right], \end{aligned} \tag{3.5}$$

where

$$
\begin{aligned}
M_0 &= \mu_2\mu_5^2(\mu_1-\mu_3)^2(\mu_2-\mu_4)^2(\rho^2+\mu_1\mu_2)^2(\rho^2+\mu_1\mu_4)^2(\rho^2+\mu_2\mu_3)^2\,,\\
M_1 &= \mu_1^2\mu_2\mu_3\mu_4\mu_5\rho^2(\mu_1-\mu_2)^2(\mu_2-\mu_4)^2(\mu_1-\mu_5)^2(\rho^2+\mu_2\mu_3)^2\,,\\
M_2 &= \mu_2\mu_3\mu_4\mu_5\rho^2(\mu_1-\mu_2)^2(\mu_1-\mu_3)^2(\rho^2+\mu_1\mu_4)^2(\rho^2+\mu_2\mu_5)^2\,,\\
M_3 &= 2\mu_1\mu_2\mu_3\mu_4\mu_5(\mu_1-\mu_3)(\mu_1-\mu_5)(\mu_2-\mu_4)(\rho^2+\mu_1^2)(\rho^2+\mu_2^2)\\
&\qquad\times(\rho^2+\mu_1\mu_4)(\rho^2+\mu_2\mu_3)(\rho^2+\mu_2\mu_5)\,,\\
M_4 &= \mu_1^2\mu_2\mu_3^2\mu_4^2(\mu_1-\mu_5)^2(\rho^2+\mu_1\mu_2)^2(\rho^2+\mu_2\mu_5)^2\,,
\end{aligned}
\tag{3.6}
$$

and

$$
\begin{aligned}
F &= \mu_1\mu_5(\mu_1-\mu_3)^2(\mu_2-\mu4)^2(\rho^2+\mu_1\mu_3)(\rho^2+\mu_2\mu_3)(\rho^2+\mu_1\mu_4)\\
&\qquad\times(\rho^2+\mu_2\mu_4)(\rho^2+\mu_2\mu_5)(\rho^2+\mu_3\mu_5)\prod_{i=1}^{5}(\rho^2+\mu_i^2)\,.
\end{aligned}
\tag{3.7}
$$

The off-diagonal part of the metric contains

$$
q = k\frac{c_2}{c_1}\frac{a_2-a_1}{a_2-a_4}\sqrt{\frac{2(a_3-a_1)(a_4-a_1)}{a_5-a_1}}\,,
\tag{3.8}
$$

and

$$
\omega_\psi = 2\frac{c_1R_1\sqrt{M_0M_1}-c_2R_2\sqrt{M_0M_2}+c_1^2c_2R_2\sqrt{M_1M_4}-c_1c_2^2R_1\sqrt{M_2M_4}}{F\sqrt{G_x}}\,,
\tag{3.9}
$$

where

$$
R_i = \sqrt{\rho^2+(z-a_i)^2}\,,\quad i=1,2,3,4,5
\tag{3.10}
$$

and $c_1, c_2 > 0$ are to be fixed in Section 3.4 for the desired physical conditions. Finally, we have

$$
\mu_i = \sqrt{\rho^2+(z-a_i)^2}-(z-a_i)\,,\quad i=1,2,3,4,5
\tag{3.11}
$$

where $a_1 < a_5 < a_4 < a_3 < a_2$.

3.2 Rod structure

We now analyse the rod structure of black Saturn at $\rho = 0$.

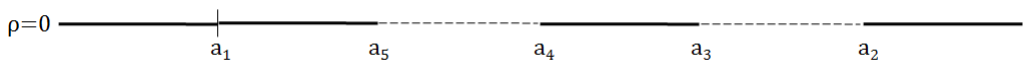

Figure 3.1: Schematic diagram of black Saturn rod structure

Figure 3.1 is a schematic diagram representing the rod structure for the black Saturn. With $t = 1$, $\phi = 2, \psi = 3$, we have:

- **Rod 1** (leftmost rod) is a semi-infinite spacelike rod at ($\rho = 0$, $z \leq a_1$) with direction $v_{(1)} = \frac{1}{\kappa_{E,1}}(0, 1, 0)$.

- **Rod 2** is a finite spacelike rod at ($\rho = 0$, $a_1 \leq z \leq a_5$) with direction $v_{(2)} = \frac{1}{\kappa_{E,2}}(0, 1, 0)$.

- **Rod 3** is a finite timelike rod at ($\rho = 0$, $a_5 \leq z \leq a_4$) with direction $v_{(3)} = \frac{1}{\kappa_3}(1, 0, \Omega_{BR})$, where Ω_{BR} is the angular velocity of the ER black ring in the ψ-direction and will be given in Section 4.3.1.

- **Rod 4** is a finite spacelike rod at ($\rho = 0$, $a_4 \leq z \leq a_3$) with direction $v_{(4)} = \frac{1}{\kappa_{E,4}}(0, 1, 0)$.

- **Rod 5** is a finite timelike rod at ($\rho = 0$, $a_3 \leq z \leq a_2$) with direction $v_{(5)} = \frac{1}{\kappa_5}(1, 0, \Omega_{BH})$, where Ω_{BH} is the angular velocity of the MP black hole in the ψ-direction and will be given in Section 4.3.1 as well.

- **Rod 6** (rightmost rod) is a semi-infinite spacelike rod at ($\rho = 0$, $z \geq a_2$) with direction $v_{(6)} = \frac{1}{\kappa_{E,6}}(0, 0, 1)$.

The surface gravities κ (2.8) of the timelike rods 3 and 5, and the Euclidean surface gravities κ_E (2.7) of the spacelike rods 1, 2, 4 and 6 are as follows:

$$\kappa_{E,1} = \frac{2(a_2 - a_4)(a_3 - a_1)}{k[c_1 c_2 (a_5 - a_1) + 2(a_2 - a_4)(a_3 - a_1)]}\,, \tag{3.12}$$

$$\kappa_{E,2} = \frac{\sqrt{2}(a_2 - a_4)\sqrt{a_3 - a_1}\sqrt{a_4 - a_1}}{k\sqrt{a_5 - a_1}[c_1(a_2 - a_4) + c_2(a_4 - a_1)]}\,, \tag{3.13}$$

$$
\begin{aligned}
\kappa_3 = \Bigg[& \big(c_1^2 c_2^2 (a_2-a_4)^2 (a_5-a_1)^2 (a_2-a_5)(a_3-a_1)(a_3-a_5)(a_4-a_1) \\
& + 4c_1 c_2 (a_2-a_4)^3 (a_3-a_1)^2 (a_2-a_5)(a_3-a_5)(a_4-a_1)(a_5-a_1) \\
& + 4(a_2-a_4)^4 (a_3-a_1)^3 (a_2-a_5)(a_3-a_5)(a_4-a_1)\big) \\
& \Big/ \big(2k^2 [c_1^2 c_2^2 (a_2-a_1)^2 (a_2-a_4)^2 (a_3-a_4)^2 (a_4-a_5)(a_5-a_1)^2 \\
& \quad - 2c_1 c_2^3 (a_2-a_1)^2 (a_2-a_4)(a_2-a_5)(a_3-a_1)(a_3-a_4) \\
& \qquad \times (a_4-a_1)(a_4-a_5)(a_5-a_1) \\
& \quad - 4c_1 c_2 (a_2-a_1)^2 (a_2-a_4)^3 (a_3-a_1)(a_3-a_4)(a_4-a_1) \\
& \qquad \times (a_4-a_5)(a_5-a_1) \\
& \quad + c_2^4 (a_2-a_1)^2 (a_2-a_5)^2 (a_3-a_1)^2 (a_4-a_1)^2 (a_4-a_5) \\
& \quad + 4c_2^2 (a_2-a_1)^2 (a_2-a_4)^2 (a_2-a_5)(a_3-a_1)^2 (a_4-a_1)^2 (a_4-a_5) \\
& \quad + 4(a_2-a_1)^2 (a_2-a_4)^4 (a_3-a_1)^2 (a_4-a_1)^2 (a_4-a_5)]\big) \Bigg]^{1/2}
\end{aligned}
\tag{3.14}
$$

$$
\kappa_{E,4} = \frac{\sqrt{a_2-a_4}\sqrt{a_2-a_5}\sqrt{a_3-a_1}\sqrt{a_3-a_5}}{k(a_3-a_4)(a_2-a_1)}\,, \tag{3.15}
$$

$$
\begin{aligned}
\kappa_5 = \Bigg[& \big[c_1^2 c_2^2 (a_2-a_3)(a_2-a_4)(a_2-a_5)(a_5-a_1)^2 \\
& + 4c_1 c_2 (a_2-a_3)(a_2-a_4)^2 (a_2-a_5)(a_3-a_1)(a_5-a_1) \\
& + 4(a_2-a_3)(a_2-a_4)^3 (a_2-a_5)(a_1-a_3)^2\big] \\
& \Big/ \big[2k^2 c_2^4 (a_2-a_1)^2 (a_2-a_5)^2 (a_3-a_1)^2 \\
& \quad + 8k^2 c_2^2 (a_2-a_1)^2 (a_2-a_3)(a_2-a_4)(a_2-a_5)(a_3-a_1)^2 \\
& \quad + 8k^2 (a_2-a_1)^2 (a_2-a_3)^2 (a_2-a_4)^2 (a_3-a_1)^2\big] \Bigg]^{1/2},
\end{aligned}
\tag{3.16}
$$

$$
\kappa_{E,6} = \frac{2(a_2-a_4)(a_3-a_1)}{k[c_1 c_2 (a_5-a_1) + 2(a_2-a_4)(a_3-a_1)]}\,. \tag{3.17}
$$

3.3 Asymptotic behaviour

The Weyl coordinates of the black Saturn solution in terms of the asymptotic coordinates [8] are

$$
\rho = \frac{1}{2} r^2 \sin 2\theta, \quad z = \frac{1}{2} r^2 \cos 2\theta\,, \tag{3.18}
$$

where we have

$$
d\rho^2 + dz^2 = r^2 (dr^2 + r^2 d\theta^2) \tag{3.19}
$$

when $r \to \infty$. Taylor expansion near the asymptotic limit of $r^2 = 2\sqrt{\rho^2 + z^2} \to \infty$ gives the asymptotic conformal factor $f \to f_{inf}$ and the asymptotic metric components:

$$f_{inf} = \frac{k^2}{r^2}\left[1 + \frac{c_1^2 c_2^2 (a_5 - a_1)^2 + 4c_1 c_2 (a_2 - a_4)(a_3 - a_1)(a_5 - a_1)}{4(a_2 - a_4)^2 (a_3 - a_1)^2}\right], \quad (3.20)$$

$$\begin{aligned} g_{11,inf} = -1 + \Big[& 2c_1^2 c_2^2 (a_5 - a_1)^2 (a_1 - a_2 - a_3 + a_4) \\ & - 8c_1 c_2 (a_2 - a_4)(a_3 - a_1)(a_3 - a_4)(a_5 - a_1) \\ & + 4c_2^2 (a_2 - a_1)^2 (a_3 - a_1)^2 \\ & - 8(a_2 - a_4)^2 (a_3 - a_1)^2 (a_1 - a_2 + a_3 - a_4)\Big] \\ & \Big/ \Big[r^2 (c_1^2 c_2^2 (a_5 - a_1)^2 + 4c_1 c_2 (a_2 - a_4)(a_3 - a_1)(a_5 - a_1) \\ & + 4(a_2 - a_4)^2 (a_3 - a_1)^2)\Big], \end{aligned} \quad (3.21)$$

$$g_{12,inf} = 0\,, \quad (3.22)$$

$$\begin{aligned} g_{13,inf} = \frac{\sin^2\theta}{r^2} \big[& 4c_1^3 c_2^2 (a_2 - a_1)(a_2 - a_4)(a_5 - a_1)^3 \\ & - 4c_1^2 c_2^3 (a_2 - a_1)(a_3 - a_1)(a_5 - a_1)^2 \\ & \qquad \times (a_1 - 2a_2 - a_3 + a_4 + a_5) \\ & + 16 c_1^2 c_2 (a_2 - a_1)(a_2 - a_4)^2 (a_3 - a_1)(a_5 - a_1)^2 \\ & + 8c_1 c_2^2 (a_2 - a_1)(a_2 - a_4)(a_3 - a_1)^2 (a_5 - a_1) \\ & \qquad \times (a_1 + a_2 + 2a_3 - 2a_4 - 2a_5) \\ & + 16 c_1 (a_2 - a_1)(a_2 - a_4)^3 (a_3 - a_1)^2 (a_5 - a_1) \\ & - 8c_2^3 (a_2 - a_1)^3 (a_3 - a_1)^3 \\ & + 16 c_2 (a_2 - a_1)(a_2 - a_4)^2 (a_3 - a_1)^3 \\ & \qquad \times (2a_1 - a_2 + a_3 - a_4 - a_5)\big] \\ & \Big/ \big[c_1^3 c_2^3 (a_5 - a_1)^3 + 6c_1^2 c_2^2 (a_2 - a_4)(a_3 - a_1)(a_5 - a_1)^2 \\ & + 12 c_1 c_2 (a_2 - a_4)^2 (a_3 - a_1)^2 (a_5 - a_1) \\ & + 8(a_2 - a_4)^3 (a_3 - a_1)^3\big], \end{aligned} \quad (3.23)$$

$$g_{22,inf} = r^2 \cos^2\theta\,, \quad (3.24)$$

$$g_{23,inf} = 0\,, \quad (3.25)$$

$$g_{33,inf} = r^2 \sin^2\theta\,. \quad (3.26)$$

Since the asymptotic conformal factor (3.20) is, to leading order, $\frac{1}{r^2}$, we demand

$$k = \frac{2(a_2 - a_4)(a_3 - a_1)}{c_1 c_2 (a_5 - a_1) + 2(a_2 - a_4)(a_3 - a_1)}\,, \tag{3.27}$$

so that the asymptotic metric takes the form

$$ds^2 = -dt^2 + dr^2 + r^2 d\theta^2 + r^2 \cos^2\theta d\phi^2 + r^2 \sin^2\theta d\psi^2\,, \tag{3.28}$$

and the solution is asymptotically flat as long as the angles ϕ and ψ have periodicities:

$$\triangle\phi = \triangle\psi = 2\pi\,. \tag{3.29}$$

3.4 Regularity and balance

The black Saturn metric components g_{tt} and $g_{\psi\psi}$ at $\rho = 0$ are found to contain a $(z - a_1)^{-1}$ divergence which implies the presence of naked conical singularities in the rod structure around $z = a_1$. To eliminate them, we set

$$c_1 = \sqrt{\frac{2(a_3 - a_1)(a_4 - a_1)}{a_5 - a_1}}\,. \tag{3.30}$$

The metric at $\rho = 0$ thus becomes completely smooth across $z = a_1$, and $\kappa_{E,1} = \kappa_{E,2}$.

To ensure a periodicity $\triangle\eta = 2\pi/\kappa_E$ of 2π for every angle in the solution, or in other words, to ensure regularity on every spacelike rod, κ_E must be equal to 1. The expressions for k and c_1 respectively given by (3.27) and (3.30) guarantee that $\kappa_{E,1} = \kappa_{E,2} = \kappa_{E,6} = 1$, i.e., $\triangle\phi = 2\pi$ for Rods 1 and 2; $\triangle\psi = 2\pi$ for Rod 6. For $\kappa_{E,4} = 1$, however, we additionally require

$$\begin{aligned} c_2 = -\sqrt{2}\Big(&\sqrt{a_2 - a_4}\sqrt{a_3 - a_1}(a_1 a_3 - a_1 a_4 - a_2 a_3 + a_2 a_4) \\ &- \sqrt{a_2 - a_5}\sqrt{a_3 - a_5}(a_1 a_2 - a_1 a_4 - a_2 a_3 + a_3 a_4)\Big) \\ &\Big/\left(\sqrt{a_2 - a_5}\sqrt{a_3 - a_1}\sqrt{a_3 - a_5}\sqrt{a_4 - a_1}\sqrt{a_5 - a_1}\right). \end{aligned} \tag{3.31}$$

It is convenient to redefine the parameter c_2 by introducing the dimensionless parameter $\overline{c}_2$ [8] as

$$\overline{c}_2 = \frac{c_2}{c_1(1 - \frac{a_4 - a_1}{a_2 - a_1})}\,, \tag{3.32}$$

and with (3.30) and (3.31), we have the balancing or equilibrium condition:

$$\begin{aligned}\overline{c}_2 = \big[&\sqrt{a_2-a_5}\sqrt{a_3-a_5}(a_1a_2-a_1a_4-a_2a_3+a_3a_4)\\ &-\sqrt{a_2-a_4}\sqrt{a_3-a_1}(a_1a_3-a_1a_4-a_2a_3+a_2a_4)\big]\\ &\Big/\left[\sqrt{a_2-a_5}\sqrt{a_3-a_5}(a_4-a_1)(a_3-a_1)\left(1-\frac{a_4-a_1}{a_2-a_1}\right)\right].\end{aligned} \tag{3.33}$$

3.5 Horizons

The metric of the spatial cross-sections of the ER black ring and MP black hole horizons can be obtained from the rod structure of black Saturn by Taylor expanding the metric components of black Saturn about $\rho = 0$, since the horizons are located at $\rho = 0$ for certain ranges of z. The Taylor expansion of the $g_{\phi\phi}$ and $g_{\psi\psi}$ components give the $g^{Hor}_{\phi\phi}$ and $g^{Hor}_{\psi\psi}$ components of the near-horizon metric, whereas that of the conformal factor gives the g^{Hor}_{zz} component.

ER black ring horizon geometry

The ER black ring horizon is located at $\rho = 0$ for $a_5 \leq z \leq a_4$. The spatial cross-section of the near-horizon metric is

$$ds^2_{BR} = \frac{2(a_4-z)(z-a_5)}{a_3-z}d\phi^2 + s^2_{BR}f(z)(a_3-z)d\psi^2 + \frac{dz^2}{(a_4-z)(z-a_5)f(z)}\,, \tag{3.34}$$

where the constant s_{BR} is, in terms of k, c_1, $\overline{c}_2$ and a_i,

$$\begin{aligned}s_{BR} = \Big[&k^2(a_4-a_5)\big[c_1^4\overline{c}_2^4(a_2-a_5)^2(a_3-a_1)^2(a_4-a_1)^2\\ &-2c_1^4\overline{c}_2^3(a_2-a_1)(a_2-a_5)(a_3-a_1)(a_3-a_4)(a_4-a_1)(a_5-a_1)\\ &+c_1^4\overline{c}_2^2(a_2-a_1)^2(a_3-a_4)^2(a_5-a_1)^2\\ &+4c_1^2\overline{c}_2^2(a_2-a_1)^2(a_2-a_5)(a_3-a_1)^2(a_4-a_1)^2\\ &-4c_1^2\overline{c}_2(a_2-a_1)^3(a_3-a_1)(a_3-a_4)(a_4-a_1)(a_5-a_1)\\ &+4(a_2-a_1)^4(a_3-a_1)^2(a_4-a_1)^2\big]\\ &\Big/\Big[(a_2-a_5)(a_3-a_5)(a_3-a_1)(a_4-a_1)\\ &\quad\times\Big(c_1^4\overline{c}_2^2(a_5-a_1)^2+4c_1^2\overline{c}_2(a_2-a_1)(a_3-a_1)(a_5-a_1)\\ &\qquad+4(a_2-a_1)^2(a_3-a_1)^2\Big)\Big]\Big]^{1/2},\end{aligned} \tag{3.35}$$

and the function $f(z)$ is

$$\begin{aligned} f(z) = 4(z-a_1)(a_2-z)(a_2-a_1)^2(a_2-a_5)(a_3-a_1)(a_3-a_5)(a_4-a_1) \\ \Big/\Big[k^2(a_4-a_5)\Big(c_1^2(a_2-z)^2(a_4-z)(a_2-a_1)^2(a_5-a_1)^2 \\ + 2c_1^2\overline{c}_2(z-a_1)(a_2-z)(a_4-z)(a_2-a_1)(a_2-a_5)(a_4-a_1)(a_5-a_1) \\ + c_1^2\overline{c}_2^2(z-a_1)^2(a_4-z)(a_2-a_5)^2(a_4-a_1)^2 \\ - 2(a_3-z)(z-a_5)(a_2-a_1)^4(a_4-a_1)^2\Big)\Big]\,. \end{aligned} \tag{3.36}$$

Note that $s_{BR} \geq 0$ and that $f(z)$ is positive for $a_5 \leq z \leq a_4$. The coordinate ψ parametrises a circle whose radius is a function of z, and the coordinates (z, ϕ) parametrise a two-sphere deformed by the presence of the MP black hole. Nevertheless, the topology of the horizon is $S^1 \times S^2$.

MP black hole horizon geometry

The MP black hole horizon is located at $\rho = 0$ for $a_3 \leq z \leq a_2$. The spatial cross-section of the near-horizon metric is

$$\begin{aligned} ds_{BR}^2 = \frac{2(z-a_3)(z-a_5)}{z-a_4}d\phi^2 + s_{BH}^2 g(z)(a_2-z)d\psi^2 \\ + \frac{(z-a_4)dz^2}{(a_2-z)(z-a_3)(z-a_5)g(z)}\,, \end{aligned} \tag{3.37}$$

where the constant s_{BH} is

$$\begin{aligned} s_{BH} = \Big[k^2(a_3-a_1)^2\big[c_1^4\overline{c}_2^4(a_2-a_4)^2(a_2-a_5)^2 \\ + 4c_1^2\overline{c}_2^2(a_2-a_1)^2(a_2-a_3)(a_2-a_4)(a_2-a_5) \\ + 4(a_2-a_1)^4(a_2-a_3)^2\big] \\ \Big/\Big[(a_2-a_3)(a_2-a_4)(a_2-a_5) \\ \times\Big(c_1^4\overline{c}_2^2(a_5-a_1)^2 + 4c_1^2\overline{c}_2(a_2-a_1)(a_3-a_1)(a_5-a_1) \\ + 4(a_2-a_1)^2(a_3-a_1)^2\Big)\Big]\Big]^{1/2}\,, \end{aligned} \tag{3.38}$$

and the function $g(z)$ is

$$\begin{aligned} g(z) = 4(z-a_1)(z-a_4)(a_2-a_1)^2(a_2-a_3)(a_2-a_4)(a_2-{}_5)(a_3-a_1)^2 \\ \Big/\Big[k^2\Big(c_1^2(a_2-z)^2(z-a_3)(a_2-a_1)^2(a_2-a_3)^2(a_5-a_1)^2 \\ + 2c_1^2\bar{c}_2(z-a_1)(z-a_3)(a_2-z)(a_2-a_1)(a_2-a_3)(a_2-a_4) \\ \times (a_2-a_5)(a_3-a_1)(a_5-a_1) \\ + c_1^2\bar{c}_2^2(z-a_1)^2(z-a_3)(a_2-a_4)^2(a_2-a_5)^2(a_3-a_1)^2 \\ + 2(z-a_4)(z-a_5)(a_2-a_1)^4(a_2-a_3)^2(a_3-a_1)^2\Big)\Big]. \end{aligned} \tag{3.39}$$

Note that $s_{BH} \geq 0$ and that $g(z)$ is positive for $a_3 \leq z \leq a_2$, so for $s_{BH} > 0$, the horizon is topologically a distorted S^3 due to rotation as well as the presence of the ER black ring.

3.6 Physical quantities

We have all we need to obtain the expressions for the physical quantities of black Saturn in terms of k, $c_1, \bar{c}_2$ and a_i.

3.6.1 Angular velocity

The directions of the timelike rod vectors in Section 3.2, namely $v_{(3)} = \frac{1}{\kappa_3}(1,0,\Omega_{BR})$ and $v_{(5)} = \frac{1}{\kappa_3}(1,0,\Omega_{BH})$, give the individual angular velocities of the ER black ring and MP black hole:

$$\begin{aligned} \Omega_{BR} = \big[2c_1(a_2-a_1)^2(a_3-a_1)(a_5-a_1) + c_1^3\bar{c}_2(a_2-a_1)(a_5-a_1)^2 \\ + \bar{c}_2(a_2-a_5)(a_4-a_1)\big] \\ \Big/\Big[2(a_2-a_1)\Big(c_1^2\bar{c}_2^2(a_2-a_5)(a_3-a_1)(a_4-a_1) \\ - c_1^2\bar{c}_2(a_2-a_1)(a_3-a_4)(a_5-a_1) \\ + 2(a_2-a_1)^2(a_3-a_1)(a_4-a_1)\Big)\Big], \end{aligned} \tag{3.40}$$

$$\begin{aligned} \Omega_{BH} = \big[c_1^2\bar{c}_2(a_5-a_1) + 2(a_2-a_1)(a_3-a_1)\big] \\ \times \big[c_1\bar{c}_2(a_2-a_4)(a_2-a_5)(a_3-a_1) - c_1(a_2-a_1)(a_2-a_3)(a_5-a_1)\big] \\ \Big/\Big[(a_2-a_1)(a_3-a_1)^2\Big(c_1^2\bar{c}_2(a_2-a_4)(a_2-a_5) \\ + 2(a_2-a_1)^2(a_2-a_3)\Big)\Big]. \end{aligned} \tag{3.41}$$

In general, $\Omega_{BR} \neq \Omega_{BH}$.

3.6.2 Temperature

The surface gravities of the timelike rods in Section 3.2, namely κ_3 (3.14) and κ_5 (3.16), give the individual temperatures of the ER black ring and MP black hole, since $T = \kappa/(2\pi)$:

$$\begin{aligned} T_{BR} = \frac{1}{4\pi k}\Big[&\sqrt{2(a_2-a_5)(a_3-a_1)(a_3-a_5)(a_4-a_1)} \\ &\times \left[2(a_1a_2+a_1a_3-a_2a_3) - c_1^2\bar{c}_2(a_5-a_1)\right] \\ &\Big/\Big[\sqrt{a_4-a_5}\Big(c_1^2\bar{c}_2^2(a_2-a_5)(a_3-a_1)(a_4-a_1) \\ &\qquad - c_1^2\bar{c}_2(a_2-a_1)(a_3-a_4)(a_5-a_1) \\ &\qquad + 2(a_2-a_1)^2(a_3-a_1)(a_4-a_1)\Big)\Big], \end{aligned} \tag{3.42}$$

$$\begin{aligned} T_{BH} = \frac{1}{4\pi k}\Big[&\sqrt{2(a_2-a_3)(a_2-a_4)(a_2-a_5)} \\ &\times \left[2(a_1^2-a_1a_2-a_1a_3+a_2a_3) + c_1^2\bar{c}_2(a_5-a_1)\right] \\ &\Big/\Big[(a_3-a_1)\Big(c_1^2\bar{c}_2^2(a_2-a_4)(a_2-a_5) \\ &\qquad + 2(a_2-a_1)^2(a_2-a_3)\Big)\Big]. \end{aligned} \tag{3.43}$$

3.6.3 Mass and angular momentum

The asymptotic metric (3.21) given in Section 3.3 allows us to compute the mass and angular momentum of black Saturn, as measured at infinity, using (2.10) and (2.11):

$$\begin{aligned} M = \frac{3\pi}{4}\Big[&c_1^4\bar{c}_2^2(a_5-a_1)^2(a_1-a_2-a_3+a_4) \\ &+ 2c_1^2\bar{c}_2^2(a_2-a_1)^2(a_3-a_1)^2 \\ &- 4c_1^2\bar{c}_2(a_2-a_1)(a_3-a_1)(a_3-a_4)(a_5-a_1) \\ &- 4(a_2-a_1)^2(a_3-a_1)^2(a_1-a_2+a_3-a_4)\Big] \\ &\Big/\left[c_1^2\bar{c}_2(a_5-a_1)+2(a_2-a_1)(a_3-a_1)\right]^2, \end{aligned} \tag{3.44}$$

$$
\begin{aligned}
J = \frac{\pi(a_2-a_1)}{(c_1^2\bar{c}_2(a_5-a_1)+2(a_2-a_1)(a_3-a_1))^3} \\
\times \Big[& c_1^4\bar{c}_2^3(a_3-a_1)(a_5-a_1)^2(a_1-2a_2-a_3+a_4+a_5) \\
& - c_1^4\bar{c}_2^2(a_2-a_1)(a_5-a_1)^3 \\
& + 2c_1^2\bar{c}_2^3(a_2-a_1)^2(a_3-a_1)^3 \\
& - 2c_1^2\bar{c}_2^2(a_2-a_1)(a_3-a_1)^2(a_5-a_1)(a_1+a_2+2a_3-2a_4-2a_5) \\
& - 4c_1^2\bar{c}_2(a_2-a_1)^2(a_3-a_1)(a_5-a_1)^2 \\
& - 4\bar{c}_2(a_2-a_1)^2(a_3-a_1)^3(2a_1-a_2+a_3-a_4-a_5) \\
& - 4(a_2-a_1)^3(a_3-a_1)^2(a_5-a_1)\Big] .
\end{aligned} \tag{3.45}
$$

3.6.4 Horizon area

The near-horizon metrics (3.34) and (3.37) given in Section 3.5 allow us to compute the individual event horizon areas of the ER black ring and MP black hole, using (2.12) and by integrating $X = z$ from one endpoint of their respective timelike rods to the other endpoint[1], giving:

$$
\begin{aligned}
A_{H,BR} = 4\pi^2 k\sqrt{\frac{2(a_4-a_5)^3}{(a_2-a_5)(a_3-a_1)(a_3-a_5)(a_4-a_1)}} \\
\times\big[2(a_2-a_1)^2(a_3-a_1)(a_4-a_1) \\
- c_1^2\bar{c}_2(a_2-a_1)(a_3-a_4)(a_5-a_1) \\
+ c_1^2\bar{c}_2^2(a_2-a_5)(a_3-a_1)(a_4-a_1)\big] \\
\Big/\big[c_1^2\bar{c}_2(a_5-a_1)+2(a_2-a_1)(a_3-a_1)\big] ,
\end{aligned} \tag{3.46}
$$

$$
\begin{aligned}
A_{H,BH} = 4\pi^2 k\sqrt{\frac{2(a_2-a_3)}{(a_2-a_4)(a_2-a_5)}}(a_3-a_1) \\
\times \frac{2(a_2-a_3)(a_2-a_1)^2+c_1^2\bar{c}_2^2(a_2-a_4)(a_2-a_5)}{2(a_2-a_1)(a_3-a_1)+c_1^2\bar{c}_2(a_5-a_1)} .
\end{aligned} \tag{3.47}
$$

It is easy to see that the expressions for temperature, mass and event horizon area are all real and positive for $a_1 < a_5 < a_4 < a_3 < a_2$ for all real c_1 and $\bar{c}_2$.

[1] Y is irrelevant here, since the near-horizon metric was obtained from the black Saturn rod structure instead of the complete black Saturn metric.

Chapter 4

The physics of black Saturn

4.1 Introduction

In this chapter, we will study the physical properties of black Saturn and how they vary with angular momentum, but not before reviewing the properties of the MP black hole and ER black ring solutions, which will be helpful for understanding the physics of black Saturn.

4.2 MP black hole and ER black ring physics

The behaviour of the MP black hole and ER black ring properties: event horizon area, angular velocity and temperature, as angular momentum squared is varied, are respectively shown in Figures 4.1 to 4.3. The graphs for the MP black hole are given by the solid black lines whereas the graphs for the ER black ring are given by the dashed black lines. We study these physical quantities against j^2 instead of j in order to better understand the near-$j = 1$ behaviour of each system.

Figure 4.1 demonstrates that as $j \to 1$, the reduced event horizon area of the MP black hole decreases and becomes 0 at $j = 1$, i.e., the solution becomes nakedly singular. This is because the horizon of the MP black hole flattens out into a pancake in the plane of rotation as its angular momentum increases [8]. Similarly, the S^2 of the fat ER black rings flattens out in the plane of rotation, and because the inner S^1 radius gets smaller while the outer S^1 radius grows, the fat rings approach the same naked ring singularity of the $j = 1$ MP solution. On the other hand, the S^2 of the thin black rings is nearly round and get smaller as $j \to 1$, thus the S^1 radius becomes much larger than the S^2 radius and the ring gets thinner.

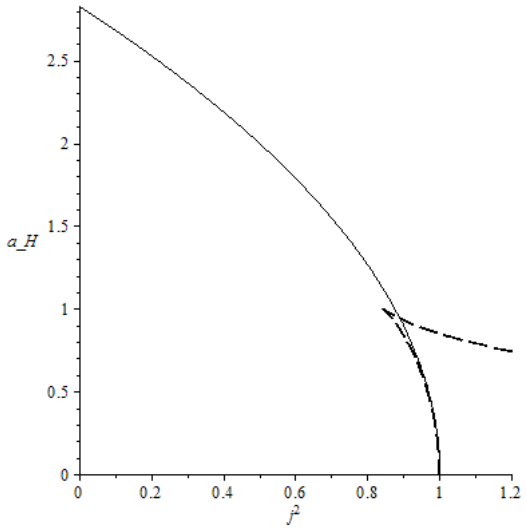

Figure 4.1: Graph of a_H against j^2

In Figure 4.2, the reduced angular velocity of the MP black hole grows linearly with reduced angular momentum because the normalisation done in Section 2.2.2 is such that $\omega_{BR} = j_{BR}$. The reduced angular velocity of the fat ER black rings also increases with reduced angular momentum, its branch approaching the graph of the MP black hole, but the thin ER black rings instead spin slower with increasing j.

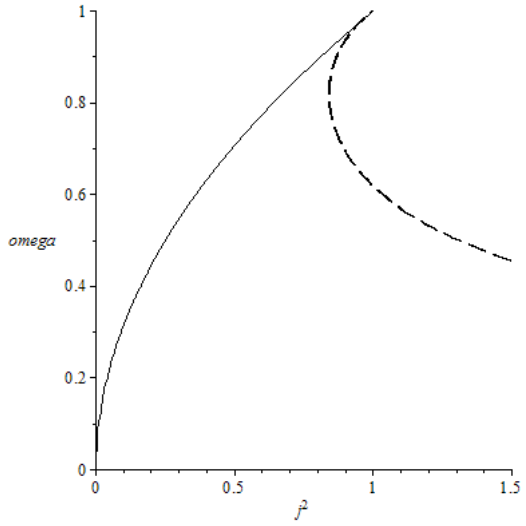

Figure 4.2: Graph of ω against j^2

Figure 4.3 shows that the MP black hole gets colder as $j \to 1$, much like the fat ER black rings, while the thin ER black rings get hotter instead.

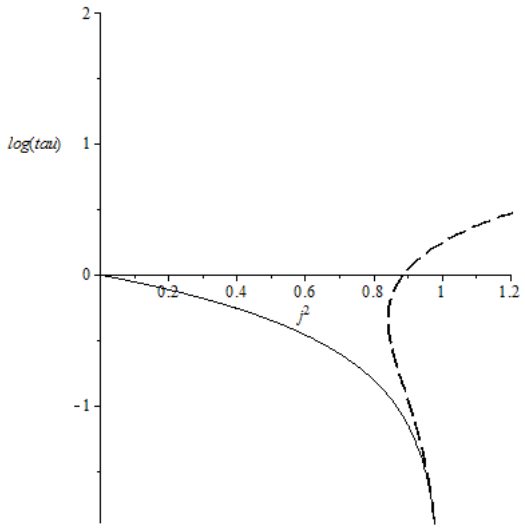

Figure 4.3: Graph of $\log \tau$ against j^2

We shall see the 'phase diagrams' of black Saturn also have 'fat' and 'thin' black ring branches which have properties mimicking those of both the MP black hole and ER black rings.

4.3 Black Saturn physics

4.3.1 Physical quantities

So far, we have been using $z = a_i$, $i = 1, 2, 3, 4, 5$, to describe the locations of the turning points or rod endpoints in the black Saturn rod structure. However, it turns out that the whole rod configuration can be shifted along the z-axis without changing the solution, which means that instead of using five dimensionful parameters, we may use three dimensionless parameters and an overall scale to describe the rod structure of the solution.

Following [8], we choose the overall scale L to be

$$L^2 = a_2 - a_1 \tag{4.1}$$

and introduce three dimensionless parameters b_i as

$$b_i = \frac{a_{i+2} - a_1}{L^2}, \quad \text{for} \quad i = 1, 2, 3 \tag{4.2}$$

such that

$$0 \leq b_3 \leq b_2 < b_1 \leq 1\,. \tag{4.3}$$

We also shift and scale the z coordinate using

$$z = L^2 \bar{z} + a_1\,, \tag{4.4}$$

such that $\bar{z}$ is dimensionless. This new parameterisation effectively corresponds to taking

$$a_1 \to 0, \quad a_5 \to b_3, \quad a_4 \to b_2, \quad a_3 \to b_1, \quad a_2 \to 1\,, \tag{4.5}$$

so from this point onwards, we shall treat the following to be true:

$$L = 1\,, \quad z = \bar{z}\,. \tag{4.6}$$

Note that $b_1 \neq b_2$, otherwise (3.33), which can now be expressed as

$$\bar{c}_2 = \frac{1}{b_2}\left[\frac{b_1 - b_2}{\sqrt{b_1(1-b_2)(1-b_3)(b_1-b_3)}} - 1\right], \tag{4.7}$$

would give $\bar{c}_2 = -\frac{1}{b_2}$, which causes the physical parameters M, J, and A_H listed below as well as k (3.27) under the new parameterisation:

$$k = \frac{1}{1 + b_2 \bar{c}_2}\,, \tag{4.8}$$

to diverge. Thus it is clear that $b_1 \neq b_2$ in order for $\bar{c}_2 \neq -\frac{1}{b_2}$.

We can now express the physical quantities of the black Saturn solution in a significantly simpler form, upon substituting the expressions for c_1 and k given by (3.30) and (4.8).

Angular velocity

$$\Omega_{BR} = \left[1 + b_2\,\bar{c}_2\right] \sqrt{\frac{b_1 b_3}{2 b_2}}\, \frac{b_3 - b_2(1-b_3)\bar{c}_2}{b_3 - b_3(b_1-b_2)\bar{c}_2 + b_1 b_2 (1-b_3)\bar{c}_2^2}\,, \tag{4.9}$$

$$\Omega_{BH} = \left[1 + b_2\,\bar{c}_2\right] \sqrt{\frac{b_2 b_3}{2 b_1}}\, \frac{b_3(1-b_1) - b_1(1-b_2)(1-b_3)\bar{c}_2}{b_3(1-b_1) + b_1 b_2 (1-b_2)(1-b_3)\bar{c}_2^2}\,. \tag{4.10}$$

Temperature

$$T_{BR} = \frac{1}{2\,\pi} \sqrt{\frac{b_1(1-b_3)(b_1-b_3)}{2 b_2 (b_2 - b_3)}}\, \frac{\left(1 + b_2\,\bar{c}_2\right)^2}{1 - (b_1 - b_2)\bar{c}_2 + \frac{b_1 b_2 (1-b_3)}{b_3}\,\bar{c}_2^2}\,, \tag{4.11}$$

,

$$T_{BH} = \frac{1}{2\,\pi} \sqrt{\frac{(1-b_2)(1-b_3)}{2(1-b_1)}}\, \frac{\left(1 + b_2\,\bar{c}_2\right)^2}{1 + \frac{b_1 b_2 (1-b_2)(1-b_3)}{b_3 (1-b_1)}\,\bar{c}_2^2}\,. \tag{4.12}$$

Mass and angular momentum

$$M = \frac{3\pi}{4}\,\frac{b_3(1-b_1+b_2) - 2b_2b_3(b_1-b_2)\bar{c}_2 + b_2\big[b_1 - b_2b_3(1+b_1-b_2)\big]\bar{c}_2^2}{b_3\big[1+b_2\bar{c}_2\big]^2}\,, \tag{4.13}$$

$$\begin{aligned} J = \frac{\pi}{b_3\big[1+b_2\bar{c}_2\big]^3}\sqrt{\frac{b_2}{2b_1b_3}}\,\Big[& b_3^2 - \bar{c}_2 b_3\Big[(b_1-b_2)(1-b_1+b_3) + b_2(1-b_3)\Big] \\ & + \bar{c}_2^2 b_2 b_3\Big[(b_1-b_2)(b_1-b_3) + b_1(1+b_1-b_2-b_3)\Big] \\ & - \bar{c}_2^3 b_1 b_2\Big[b_1 - b_2b_3(2+b_1-b_2-b_3)\Big]\Big]\,. \end{aligned} \tag{4.14}$$

Horizon area

$$A_{H,BR} = 4\pi^2\sqrt{\frac{2b_2(b_2-b_3)^3}{b_1(b_1-b_3)(1-b_3)}}\;\frac{1-(b_1-b_2)\bar{c}_2 + \frac{b_1b_2(1-b_3)}{b_3}\,\bar{c}_2^2}{\big(1+b_2\,\bar{c}_2\big)^2}\,, \tag{4.15}$$

$$A_{H,BH} = 4\pi^2\sqrt{\frac{2(1-b_1)^3}{(1-b_2)(1-b_3)}}\;\frac{1+\frac{b_1b_2(1-b_2)(1-b_3)}{b_3(1-b_1)}\,\bar{c}_2^2}{\big(1+b_2\,\bar{c}_2\big)^2}\,. \tag{4.16}$$

Now, using (2.32), the fixed mass reduced parameters for the quantities in Section 4.3.1 can be found easily, albeit they are too lengthy to be presented explicitly in this thesis.

Komar integrals

We introduce Komar integrals [8] which measure mass and angular momentum not at infinity but on the horizon H_i of each black hole in the black Saturn system.

In 5D spacetime, the Komar mass, i.e., the mass contained within the surface of an event horizon, can be given in terms of metric components [8] such that:

$$M_{Komar,i} = \frac{3}{32\pi}\int_{H_i} dz d\phi d\psi \frac{1}{\sqrt{-\mathrm{det}g}} g_{zz}g_{\phi\phi}[-g_{\psi\psi}\partial_\rho g_{tt} + g_{t\psi}\partial_\rho g_{t\psi}]\,, \tag{4.17}$$

and therefore, for the black Saturn solution,

$$M_{Komar,BR} = \frac{3\pi}{4}\,\frac{b_2[1-(1-b_2)\bar{c}_2][b_3 - b_3(b_1-b_2)\bar{c}_2 + b_1b_2(1-b_3)\bar{c}_2^2}{b_3(1+b_2\bar{c}_2}\,, \tag{4.18}$$

$$M_{Komar,BH} = \frac{3\pi}{4}\frac{b_3(1-b_3)+b_1b_2(1-b_2)(1-b_3)\bar{c}_2^2}{b_3(1+b_2\bar{c}_2)}\,. \tag{4.19}$$

We find that

$$M = M_{Komar,BR} + M_{Komar,BH}\,, \tag{4.20}$$

even in the presence of a conical singularity, that is, even without imposing (3.30). Recall that M refers to the total mass of black Saturn measured at infinity.

The Komar angular momentum, i.e., the angular momentum contained within the surface of an event horizon, is also called the 'intrinsic' angular momentum of a black hole. It is given by [8]:

$$J_{Komar,i} = -\frac{1}{16\pi}\int_{H_i} dz d\phi d\psi \frac{1}{\sqrt{-\mathrm{det}g}} g_{zz}g_{\phi\phi}[-g_{\psi\psi}\partial_\rho g_{t\psi} + g_{t\psi}\partial_\rho g_{\psi\psi}]\,, \tag{4.21}$$

and therefore, for the black Saturn solution,

$$\begin{aligned} J_{Komar,BR} = \pi\sqrt{\frac{b_2}{2b_1b_3}}\,\frac{1}{b_3(1+b_2\bar{c}_2)^3}[b_3 - b_2(b_1-b_3)\bar{c}_2 + b_1b_2(1-b_2)\bar{c}_2^2] \\ \times [b_3 - b_3(b_1-b_2)\bar{c}_2 + b_1b_2(1-b_3)\bar{c}_2^2]\,, \end{aligned} \tag{4.22}$$

$$J_{Komar,BH} = -\pi\sqrt{\frac{b_1b_2}{2b_3}}\,\frac{\bar{c}_2[b_3(1-b_1)+b_1b_2(1-b_2)(1-b_3)\bar{c}_2^2]}{b_3(1+b_2\bar{c}_2)^2}\,. \tag{4.23}$$

We also find that

$$J = J_{Komar,BR} + J_{Komar,BH}\,, \tag{4.24}$$

even without balancing the solution, that is, even without imposing (3.33). Recall that J refers to the total angular momentum of black Saturn measured at infinity.

Smarr relations

The Smarr formula

$$\frac{2}{3}M_{Komar,i} = T_iS_i + \Omega_iJ_{Komar,i} \tag{4.25}$$

is a mathematical identity relating the physical quantities of a black hole measured at its horizon and is obeyed by the MP black hole [13] and the ER black ring [2], the individual black objects constituting the black Saturn system, as well as multiple-black-hole systems in general [14]. S is the entropy of a black hole which black hole thermodynamics has established is proportional to event horizon area: $S = A_H/4$ [17]. Hence, Ω, T, M_{Komar}, J_{Komar} and A_H are all inextricably related to one another via the Smarr relation.

4.3.2 Black Saturn: $J_{Komar,BH} = 0$ configuration

In this section, we study the subfamily of black Saturn where the intrinsic or Komar angular momentum of the MP black hole vanishes: $J_{Komar,BH} = 0$, a property that is met when $\bar{c}_2 = 0$, as can be deduced easily from (4.23). This choice will prove to be strategic in Section 4.3.3.

With $\bar{c}_2 = 0$, we can solve for b_3 using (4.7): there will be two solutions, namely:

$$(1) \qquad b_3 = \frac{1}{2b_1(1-b_2)}\Big[b_1 - b_1 b_2 + b_1^2 - b_1^2 b_2 - \sqrt{b_1(1-b_2)(b_1 + 4b_2^2 - 9b_1 b_2 + 2b_1^2 + 2b_1^2 b_2 + b_1^3 - b_1^3 b_2)}\Big], \quad (4.26)$$

$$(2) \qquad b_3 = \frac{1}{2b_1(1-b_2)}\Big[b_1 - b_1 b_2 + b_1^2 - b_1^2 b_2 + \sqrt{b_1(1-b_2)(b_1 + 4b_2^2 - 9b_1 b_2 + 2b_1^2 + 2b_1^2 b_2 + b_1^3 - b_1^3 b_2)}\Big]. \quad (4.27)$$

but only one solution (4.26) satisfies the inequality constraint $0 < b_3(b_1, b_2) < b_2 < b_1 < 1$. Finally, in order to obtain a 1-parameter family of solutions for effective illustration of the physics of black Saturn, we must further fix a physical quantity. Following [8], we have chosen to fix either the reduced event horizon area of the ER black ring $a_{H,BR}$ or the reduced event horizon area of the MP black hole $a_{H,BH}$, as we shall see below.

4.3.3 Fixed $a_{H,BR}$

In Figure 4.1, we saw that the reduced event horizon area $a_{H,BR}$ of the ER black ring takes values $0 < a_{H,BR} \leq 1$, thus $a_{H,BR}$ can be fixed at any value between 0 (inclusive) and 1 (exclusive), and the MP black hole can be 'grown' at the centre of the ER black ring, i.e., starting with a given value of fixed $a_{H,BR}$ with a nakedly singular MP black hole in the centre, $a_{H,BH}$ is gradually increased to give a black Saturn system. The cases of $a_{H,BR} = 0$ and $a_{H,BR} = 1$ will be addressed later on in this section. Note that the graphs for the MP black hole (solid black line) and the ER black ring (dashed black line) are included for comparison in most, if not all, the graphs in this section.

Non-uniqueness

The graphs shown in Figures 4.4 to 4.8 of reduced event horizon area a_H against reduced angular momentum-squared j^2 for the black Saturn solution

have two branches: an upper and lower branch, for any value $0 < a_{H,BR} \leq 1$. As such, for each $a_{H,BR}$, a finite range of values of j^2 admit two solutions with different total a_H, clearly exhibiting violation of the uniqueness theorem. However, the phenomenon of non-uniqueness does not stop at being discrete at certain regimes. Instead, the balanced black Saturn configuration exhibits two-fold continuous non-uniqueness because the total mass M and angular momentum J of the system can be distributed continuously between the MP black hole and the ER black ring to resemble other 5D black hole solutions when viewed at infinity. In particular, the continuous set of black Saturn systems whose MP black hole and ER black ring counter-rotate to give zero total angular momentum at infinity is asymptotically identical to the 5D Tangherlini solution. Black holes in 5D thus have huge degeneracies.

We can theoretically plot graphs of reduced event horizon area against angular momentum-squared for a continuous set of $a_{H,BR}$ values between 0 and 1 to accurately illustrate continuous non-uniqueness for certain regimes of j^2, but since this is highly impractical, Figure 4.4 uses only a representative sample of black Saturn configurations: $a_{H,BR} = 0.10, 0.20, 0.30, 0.50, 0.90$ to show non-uniqueness. For instance, there exist ten different black Saturn solutions with $j^2 = 0.85$.

The reason for the two branches of the black Saturn is because the MP black hole can be 'grown' from either the thin ring or the fat ring branch of the ER black ring to give the balanced black Saturn system. This can be more clearly seen for black Saturn configurations with larger values of $a_{H,BR}$: $a_{H,BR} = 0.50, 0.60, 0.70, 0.80, 0.90, 0.95$, in Figures 4.5 and 4.6, where the branches of the black Saturn graphs are seen to 'originate' from the respective branches of the ER black ring graph at various values of j^2. Since $J_{Komar,BH} = 0$, the MP black hole contributes no angular momentum, and hence j^2 decreases as the MP black hole grows, until the cusp of the curve is reached.

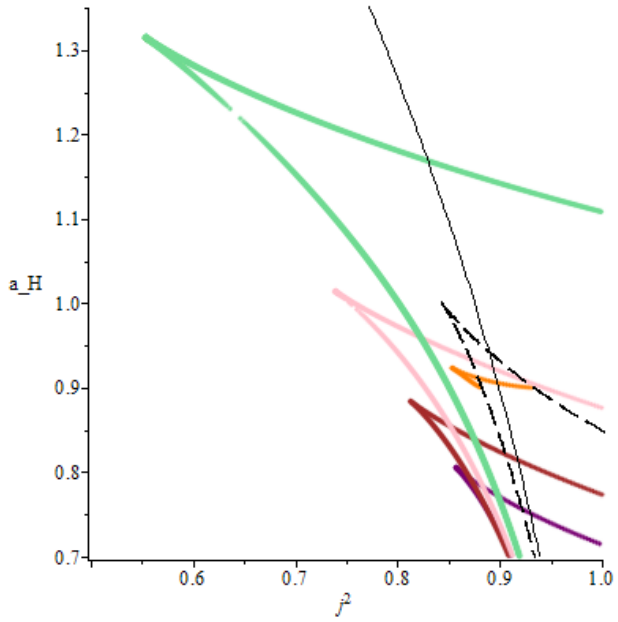

Figure 4.4: Graphs of total a_H against j^2 for a range of fixed $a_{H,BR}$ values: 0.10 (teal), 0.20 (pink), 0.30 (brown), 0.50 (purple), 0.90 (orange).

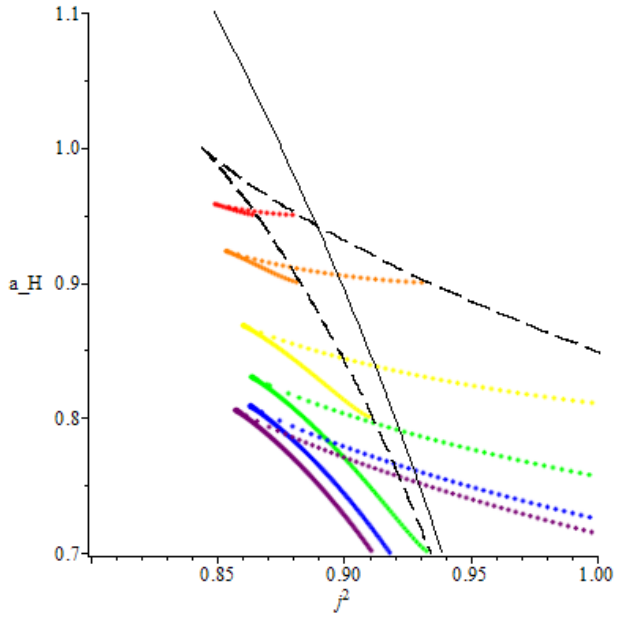

Figure 4.5: Graphs of total a_H against j^2 for large $a_{H,BR}$ values: 0.50 (purple), 0.60 (dark blue), 0.70 (green), 0.80 (yellow), 0.90 (orange), 0.95 (red).

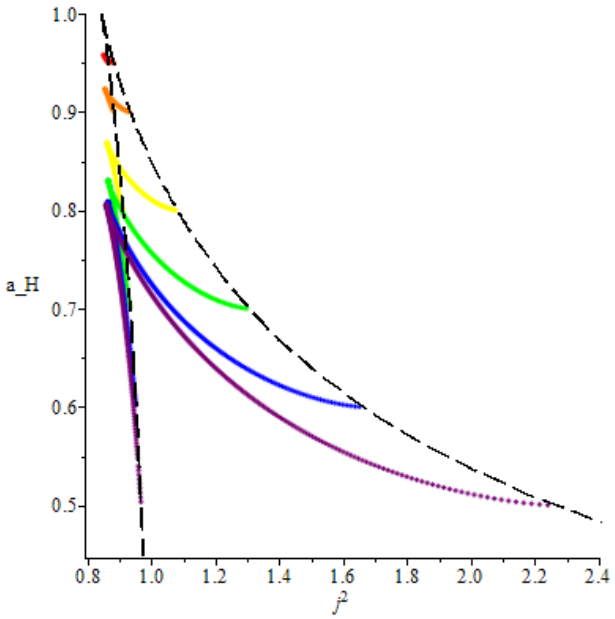

Figure 4.6: Graphs of total a_H against j^2 for large $a_{H,BR}$ values: 0.50 (purple), 0.60 (dark blue), 0.70 (green), 0.80 (yellow), 0.90 (orange), 0.95 (red). The MP black hole is being 'grown' at the centre of the ER black rings.

The same is true for black Saturn configurations with smaller values of $a_{H,BR}$: $a_{H,BR} = 0.05, 0.10, 0.20, 0.30, 0.40$, in Figures 4.7 to 4.8, though the MP black hole starts 'growing' only at much larger values of j^2, as seen from the point at which the tails of the black Saturn graphs end on the tails of the ER black ring graphs. For such small fixed values of $a_{H,BR}$, the MP black hole is allowed to grow very large, and the black Saturn phases dominate the ER black ring branches entropically.

It can be seen that increasing the fixed values of $a_{H,BR}$ causes the black Saturn phase to become smaller. When fixed $a_{H,BR} = 1$ is reached, there are no black Saturn solutions, because growing the MP black hole from the ER black ring decreases j, and for the black ring with $j = \sqrt{\frac{27}{32}}$ and $a_{H,BR} = 1$, there are no black ring solutions with less angular momentum. However, it is possible to fix $a_{H,BR} = 0$; this describes a nakedly singular black ring rotating around an MP black hole which is also rotating as it is being dragged along by the ring singularity. We will see this graph in Section 4.3.4.

It is interesting to note that the lowest of all the black Saturn graphs is that of $a_{H,BR} = 0.50$, i.e., as $a_{H,BR}$ increases from 0, the black Saturn reduced event horizon area a_H decreases dramatically until it reaches a minimum or a turning point, $a_{H,BR} = 0.50$, before increasing gradually to $a_H = 1$.

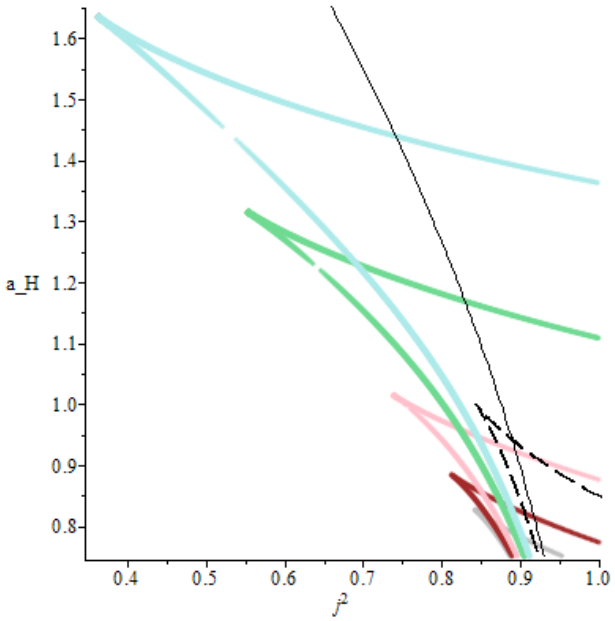

Figure 4.7: Graphs of total a_H against j^2 for small $a_{H,BR}$ values: 0.05 (light blue), 0.10 (teal), 0.20 (pink), 0.30 (brown), 0.40 (grey).

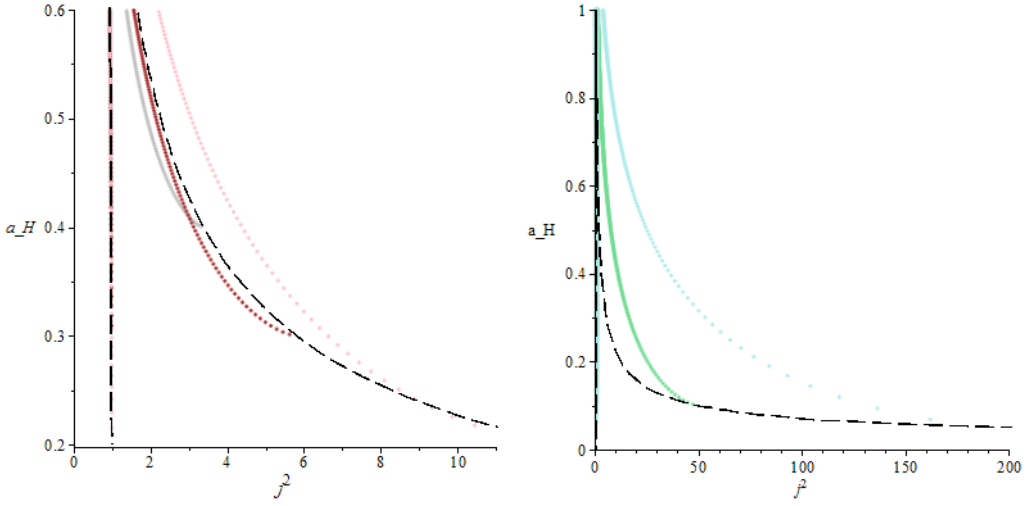

Figure 4.8: Graphs of total a_H against j^2 for small $a_{H,BR}$ values: 0.05 (light blue), 0.10 (teal), 0.20 (pink), 0.30 (brown), 0.40 (grey). The MP black hole is being 'grown' at the centre of the ER black rings.

Frame-dragging

The graph of reduced angular velocity ω against reduced angular momentum-squared j^2 in Figure 4.9 for the black Saturn solution includes ω_{BR} as well as ω_{BH}, the former being above the latter, and both the ω_{BR} and ω_{BH} graphs have a fat ring branch and a thin ring branch.

It is interesting to note that the reduced angular velocity ω_{BH} of the MP black hole is non-zero, i.e., the MP black hole is rotating, despite having fixed its intrinsic angular momentum $J_{Komar,BH} = 0$, a strategic choice that gives the cleanest possible illustration of the physical phenomenon of gravitational frame-dragging: an effect of General Relativity whereby the azimuthally rotating ER black ring drags the spacetime surrounding it, causing the MP black hole horizon to rotate and ω_{BH} to follow the behaviour of ω_{BR}. This interpretation is reasonable, since for any value of j^2, the angular velocity of the MP black hole ω_{BH} is always smaller than that of the ER black ring ω_{BR}.

Note that the reduced angular velocity ω_{BH} of the MP black hole is higher along its fat ring branch than its thin ring branch, because a thin ring with large S^1 radius rotating relatively slowly can hardly be felt by the MP black hole in the centre, whereas a flattened-out fast-rotating fat ring with small S^1 radius drags spacetime around much more significantly [8]. We imagine the frame-dragging effect to be very small when the ER black ring is very far from the MP black hole, i.e., (i) the larger the MP black hole grows (in the direction of decreasing j^2) or, in fact, (ii) the faster the MP black hole spins and thus the more it flattens out in the plane of rotation, then the closer it is to the ER black ring and the larger its angular velocity.

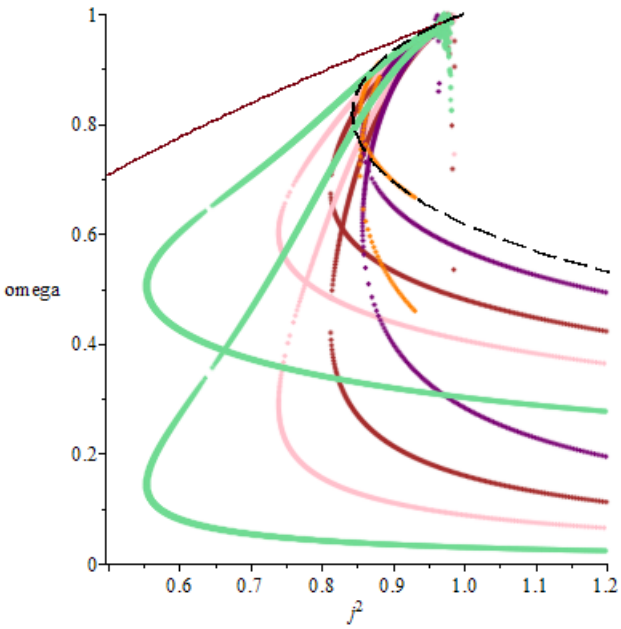

Figure 4.9: Graphs of ω_{BR} and ω_{BH} against j^2 for a range of fixed $a_{H,BR}$ values: 0.10 (teal), 0.20 (pink), 0.30 (brown), 0.50 (purple), 0.90 (orange).

Temperature

The graph of the logarithm of reduced temperature $\log(\tau)$ against angular momentum-squared j^2 in Figure 4.10 for the black Saturn solution includes $\log(\tau_{BR})$ as well as $\log(\tau_{BH})$, the former being below the latter, and both the $\log(\tau_{BR})$ and $\log(\tau_{BH})$ graphs have a fat ring branch and a thin ring branch.

Figure 4.11 shows only the graph of $\log(\tau_{BR})$ against j^2 whereas Figure 4.12 shows only the graph of $\log(\tau_{BH})$ against j^2. As the fixed value of $a_{H,BR}$ is decreased, the MP black hole can take a larger and larger range of angular momentum, over which its temperature becomes more or less constant.

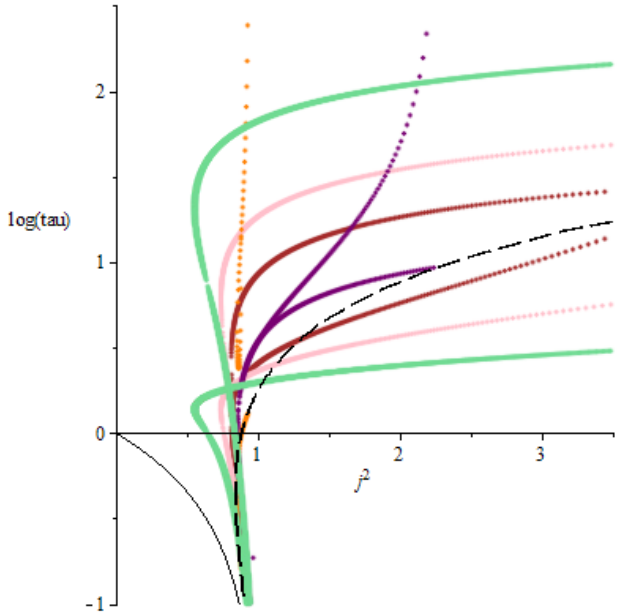

Figure 4.10: Graphs of $\log(\tau_{BR})$ and $\log(\tau_{BH})$ against j^2 for a range of fixed $a_{H,BR}$ values: 0.10 (teal), 0.20 (pink), 0.30 (brown), 0.50 (purple), 0.90 (orange).

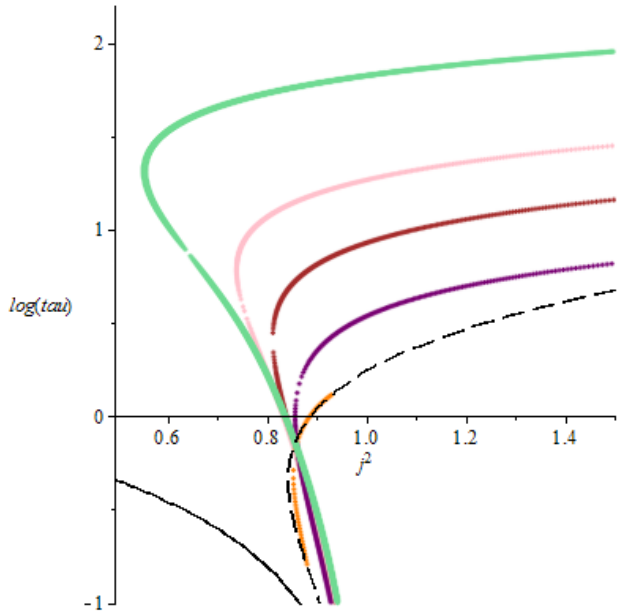

Figure 4.11: Graphs of $\log(\tau_{BR})$ against j^2 for a range of fixed $a_{H,BR}$ values: 0.10 (teal), 0.20 (pink), 0.30 (brown), 0.50 (purple), 0.90 (orange).

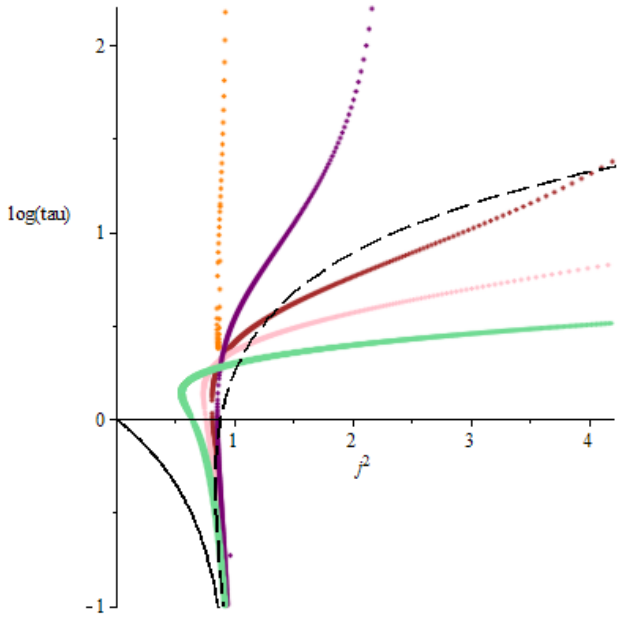

Figure 4.12: Graphs of $\log(\tau_{BH})$ against j^2 for a range of fixed $a_{H,BR}$ values: 0.10 (teal), 0.20 (pink), 0.30 (brown), 0.50 (purple), 0.90 (orange).

4.3.4 Fixed $a_{H,BH}$

In this section, we fix the reduced event horizon area $a_{H,BH}$ of the MP black hole instead, remembering that the intrinsic angular momentum of the MP black hole is still 0. By doing so, we are 'growing' an ER black ring around MP black holes with different horizon areas instead. However, a balanced black ring cannot exist for arbitrarily small angular momentum while keeping the configuration in equilibrium, thus the black ring must grow from a nakedly singular ring around an MP black hole, shown by the dotted curve, which is essentially the black Saturn graph for $a_{H,BR} = 0$.

Figure 4.13 displays a representative sample of black Saturn graphs with $a_{H,BH} = \sqrt{\frac{1}{10}}, \sqrt{\frac{7}{10}}, \sqrt{\frac{3}{2}}, \sqrt{3}, \sqrt{6}$. Every graph has two branches, including the graph for large $a_{H,BH} = \sqrt{6}$, which we zoom into in Figure 4.14 to ascertain that this is true. Black Saturn solutions with large $a_{H,BH}$ can reach very small values of j, but we note that for $\bar{c}_2 = 0$, j will never reach 0 because, given (4.24) and the fact that $J_{Komar,BR}$, $J_{Komar,BH}$ cannot *both* be 0 (the system must rotate to be balanced), $j = 0$ requires that the MP black hole and ER black ring are counter-rotating, which is impossible: $\bar{c}_2 = 0$ gives a non-rotating MP black hole with $J_{Komar,BH} = 0$ (4.23). We also note that black Saturn solutions with small $a_{H,BH}$ approach the ER black ring graph and eventually reduce to it when $a_{H,BH} = 0$.

While the thin ring branch of the black Saturn graphs extends to infinity, the fat ring phase stops upon intersecting with the graph of $a_{H,BR} = 0$. The large j-tails show that balanced thin-ring Saturn configurations can have very large entropies [8] within the range $0 < a_{H,BH} < 2\sqrt{2}$, where $2\sqrt{2}$ is the y-intercept of the MP graph given by the solid black line, i.e. it is the reduced event horizon area of the 5D Tangherlini solution. This means that for any value of angular momentum, there exists black Saturn configurations with total reduced event horizon area arbitrarily close to $2\sqrt{2}$.

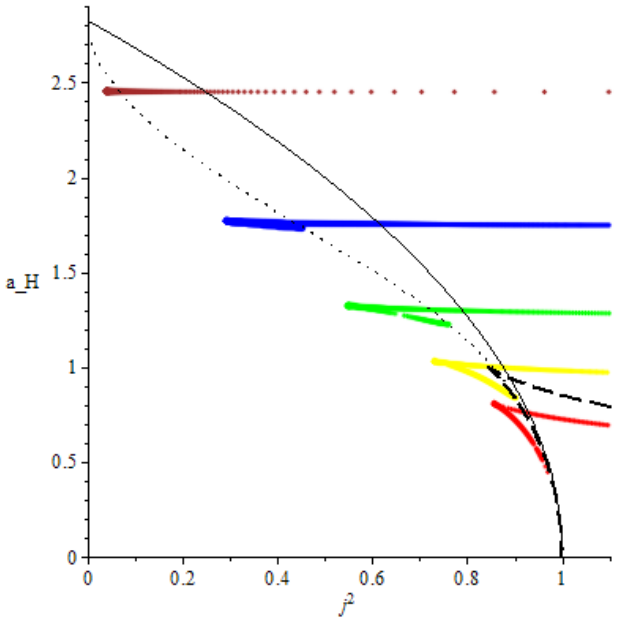

Figure 4.13: Graphs of total a_H against $j^2$for a range of fixed $a_{H,BH}$ values: $\sqrt{\frac{1}{10}}$ (red), $\sqrt{\frac{7}{10}}$ (yellow), $\sqrt{\frac{3}{2}}$ (green), $\sqrt{3}$ (blue), $\sqrt{6}$ (brown).

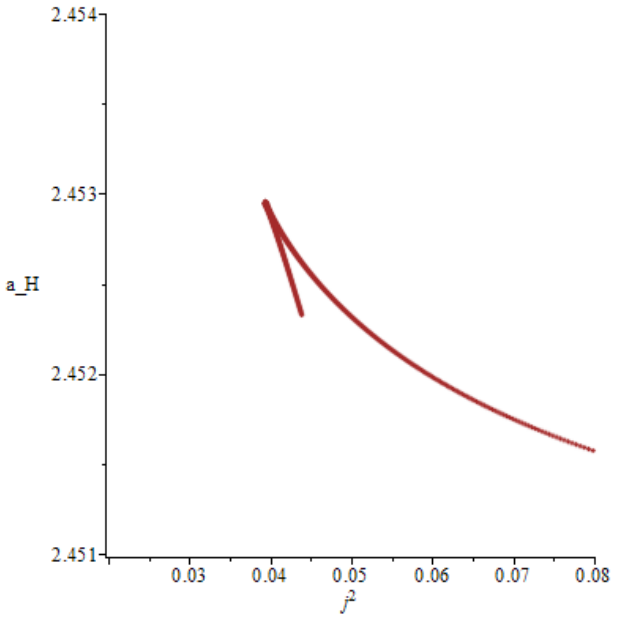

Figure 4.14: Cusp of graph of total a_H against j^2 for $a_{H,BH} = \sqrt{6}$

Chapter 5

Conclusion

5.1 Overview

In this thesis, we have presented and analysed an exact regular (4+1)-dimensional asymptotically flat multiple-black-hole vacuum solution known as the black Saturn: a Myers-Perry black hole surrounded by an Emparan-Reall black ring balanced by rotation in the plane of the ring, i.e., S^1 rotation. Interesting physical properties such as non-uniqueness and frame-dragging have been studied and can be summarised as follows:

- The uniqueness theorem is violated in higher-dimensional spacetime when dealing with stationary solutions alongside static solutions. The black Saturn solution contributes greatly to the non-uniqueness of (4+1)-dimensional black holes due to the possibility of continuously distributing mass and angular momentum between the two black objects constituting black Saturn. The solution thus exhibits two-fold continuous non-uniqueness with discrete non-uniqueness for ranges of angular momentum admitting both thin and fat black Saturn solutions.

- Rotational frame-dragging is manifested in the gravitational interaction between the MP black hole and ER black ring of the black Saturn solution. While the phenomenon is most cleanly illustrated with the MP black hole having non-zero angular velocity ω_{BH} despite having zero intrinsic angular momentum $J_{Komar,BH}$, there are other ways to study frame-dragging, which we elaborate upon below.

5.2 Outlook

The focus of this thesis has been the study of a black Saturn system comprised of an MP black hole and an ER black ring with rotation exclusively in the same direction (identical signs of angular velocities) and in the same plane (in the S^1 or azimuthal ψ-direction). Clearly, the system can be generalised in several ways:

- There are no restrictions stating that the MP black hole and ER black ring must be co-rotating to maintain balance. Since they have independent rotation parameters, they may *counter-rotate* in the same plane to produce *countering frame-dragging effects*, that is, the intrinsic angular momentum $J_{Komar,BH}$ of the MP black hole can be tuned such that it 'cancels' the effect of dragging caused by the ER black ring surrounding it. This gives a solution with the MP black hole having zero angular velocity ω_{BH} despite having non-zero intrinsic angular momentum $J_{Komar,BH}$ [8].

- The MP black hole and ER black ring may also *rotate in orthogonal planes*. In such a scenario, on top of rotational dragging of the black ring on the black hole, we expect there to be rotational dragging of the black hole on the black ring, i.e., a ϕ-rotating MP black hole should result in a ψ-rotating ER black hole having non-vanishing angular velocity on the S^2. This produces a *coupling* effect with regards to the frame-dragging between the two black objects of the black Saturn system, since the rotation of one body causes the other body to rotate, which in turn affects the rotation of the former body.

- The highest level of generalisation for the black Saturn system involves *doubly spinning MP black holes and doubly spinning MP black rings*, the solution for which may be obtained using the techniques in [15]. It must be checked that all possible singularities can be eliminated, after which the physics of the system can be analysed.

Also, while the black Saturn system in this thesis is neutrally charged, the following extensions are possible:

- Adding *non-conserved dipole charge(s)* [16] to the ER black ring in the black Saturn system will give a dipole black Saturn solution.

- Adding *conserved charge(s)* to the vacuum black Saturn solution.

The black Saturn system is an example of a system at classical equilibrium, where the objects constituting it generally having different temperatures (and angular velocities). It will be interesting to impose *thermodynamic equilibrium* and find the phases for so-called metastable black Saturns

[18], which form a one-parameter family of solutions with only discrete non-uniqueness [14], as opposed to the continuous family of black Saturns we studied earlier.

Lastly, we note that the non-uniqueness of the black Saturns studied in this thesis is two-fold because there are two free dimensionless parameters in the solution, a reduction from the original six: b_1, b_2, b_3 (where $0 \leq b_3 \leq b_2 < b_1 \leq 1$), the scale L and the parameters c_1 and c_2 - by fixing c_1 (3.30), rescaling c_2 to introduce $\overline{c}_2$ (3.32, 4.7), and fixing the conserved asymptotic quantities mass M and angular momentum J. Generalising the ER black ring of the black Saturn system to multiple rings involves more free dimensionless parameters, such that a system of n black objects possesses $2(n-1)$-fold continuous non-uniqueness [8].

Bibliography

[1] S. W. Hawking, *Black holes in General Relativity*, Commun. Math. Phys. 25 (1972) p. 152-166.

[2] R. Emparan and H. S. Reall, *A rotating black ring in five dimensions*, Phys. Rev. 88 (2002) 101101 [arXiv:hep-th/0110260].

[3] M. Heusler, *Black hole uniqueness theorems*, Cambridge University Press (1996).

[4] G. W. Gibbons, Daisuke Ida and Tetsuya Shiromizu, *Uniqueness and non-uniqueness of static black holes in higher dimensions*, Phys. Rev. Lett. 89 (2002) 041101 [arXiv:hep-th/0206049].

[5] T. Harmark, V. Niarchos and N. A. Obers, *Instabilities of black strings and branes*, Class. Quant. Grav 24 (2007) R1-R90 [arXiv:hep-th/0701022].

[6] S. D. Majumdar, *A class of exact solutions of Einstein's field equations*, Phys. Rev. 72, 390 (1947).

[7] D. Kramer and G. Neugebauer, *The superposition of two Kerr solutions*, Phys. Lett. A. 75, 4 (1980) p. 259-261.

[8] H. Elvang and P. Figueras, *Black Saturn*, (2007) [arXiv:hep-th/0701035v2].

[9] T. Harmark, *Stationary and axisymmetric solutions of higher-dimensional general relativity*, Phys. Rev. D. 70 (2004) 124002 [arXiv:hep-th/0408141].

[10] R. Emparan and H. S. Reall, *Generalized Weyl solutions*, Phys. Rev. D. 65 (2002) 084025 [arXiv:hep-th/0110258].

[11] K. Hong, *Black rings in five dimensions*, National University of Singapore (2013).

[12] Image adapted from The American Society of Mechanical Engineers, *Optimum shape of constant stress toroidal shells* (2013) [pressurevesseltech.asmedigitalcollection.asme.org/article.aspx?articleid=1672018].

[13] R. C. Myers and M. J. Perry, *Black holes in higher dimensional spacetimes*, Annals Phys. 172, 304 (1986).

[14] H. Elvang, R. Emparan and P. Figueras, *Phases of five-dimensional black holes*, [arXiv:hep-th/0702111].

[15] A. A. Pomeransky and R. A. Sen'kov, *Black ring with two angular momenta*, [arXiv:hep-th/0612005].

[16] R. Emparan, *Rotating circular strings, and infinite non-uniqueness of black rings*, JHEP 0403, 064 (2004) [arXiv:hep-th/0402149].

[17] N. Altamirano, D. Kubizňák, R. B. Mann and Z. Sherkatghanad, *Rotating circular strings, and infinite non-uniqueness of black rings*, JHEP 0403, 064 (2004) [arXiv:hep-th/0402149].

[18] J. Evslin and C. Krishnan, *Metastable black Saturns*, (2008) [arXiv:hep-th/0804.457v3].